ANAHEIM

ANAHEIM

Session J—AESF & SFSJ III

'93

AESF

SURFIN®

International Technical Conference Proceedings

June 21–24, 1993

SUR/FIN® '93

American Electroplaters and Surface Finishers Society, Inc.
80th Annual Conference—Anaheim

Session J
AESF & SFSJ III

Understanding and Controlling Electroplating 405
David Kahn, AMP, Inc., Harrisburg, PA

Advanced Surface Finishing Technology for Electronic Applications 421
Dr. Tetsuya Osaka, Waseda University, Tokyo, Japan

Anodic Oxide Films on Aluminum: Structure and New Applications 425
Dr. Nobuyoshi Baba, Metropolitan University, Tokyo, Japan

Environmental Effects on Electronic Materials 433
B.J. Rickett and Prof. J.H. Payer, Case Western Reserve University, Cleveland, OH

Printed by AESF Press

UNDERSTANDING AND CONTROLLING ELECTROPLATING

David Kahn
Corporate Technology
AMP Incorporated
P. O. Box 3608, Harrisburg PA 17105-3608

Abstract

We do not understand enough of plating bath chemistry to generate a quantitative parametric model. Nonetheless, we can construct empirical multivariate, quantitative models to predict the change in plating structure(responses) with changing plating bath parameters(factors) using only a limited number of designed experimental runs. These models can then be used either to vary the plating factors to obtain a desired response(s) or to detect changes in plating factors or a change in the underlying model from changes in the plating responses. Two of these methods, principal component analysis(PCA) and partial least-squares in latent variables(PLS), will be illustrated; and their adaptation to general multivariate process control will be discussed.

Introduction

In spite of the fact that electroplating has been an important technology in all parts of the world for many years, our understanding of this process is still very imperfect. Some reasons for this are the complicated reactions at the double layer between the metal cathode and the electrolyte, the nonlinearity of the bath reactions, the fact that baths are operated far from equilibrium, the self organization properties of the bath and the multivariate interactions that are possible. In many instances, the baths in use are proprietary, so that we are prevented from even knowing the bath contents. For any and all of these reasons, a quantitative parametric model of the bath chemistry does not exist for any commercial plating bath.

Nevertheless, a multivariate, quantitative model of the electroplating bath, is necessary if we are to understand and control this important technology. Fortunately, we do not lack for data on the plating bath parameters(factors) and the corresponding plating characteristics(responses). These data can usually be obtained from previous production runs for an old bath or from designed experimental runs for a new bath. The problem is to turn these data into useful information.

The plating bath factors used in a designed experiment of N runs may be represented as elements of a matrix of N rows(samples) and K columns(factors). Similarly the corresponding plating responses may be represented as a matrix with the same N rows and P columns

may be represented as a matrix with the same N rows and P columns corresponding to the P plating responses that are measured for each run. The 16 by 11 factor(X) matrix for a nickel process variation study for a two level fractional factorial Plackett-Burman designed experiment is shown in Table I. A plus one refers either to a high value of a plating factor or to one type of anion. A minus one corresponds to a low value of the same plating factor or to a different anion. If the two factor interactions are included, this matrix becomes a 16 by 66 matrix. The original and corresponding centered and scaled 16 by 9 response(Y) matrices are shown in Table II. The values of the plating factors used in these runs are deliberately chosen to be somewhat outside the normal operating limits to ensure that any possible factor combination that may arise during operation of the bath has been included in the model. The variations in the responses in Table II due to the change in plating factors are obvious and our first step is to look for quantitative relations between them.

The measured components from each row of the response matrix specify a point in the P dimensional response space. The arrangement of these N points in this space reflects the relations between the responses and will be discussed in more detail below. Although it is very difficult to visualize patterns in a space with more than three dimensions, the techniques described below can be used to "project" these points in sample space onto a lower dimensional space.[1] In many instances it is convenient to project these points in hyperspace onto two dimensional planes, which act as windows into the hyperspace.

Since the plating responses are the result of a multivariate process and may be correlated in ways that are unknown to the plating engineer, separating these results into a smaller number of uncorrelated components using principal component analysis(PCA) is an important first step in developing a model for the plating process. After these components are identified, our next task is to relate these plating response components to the plating bath factors using partial least-squares regression(PLS), thereby creating a quantitative model of the plating process. If the plating factors and responses arise from the same underlying model, we will obtain a regression relation that is robust and can be used with confidence over a wide range of plating conditions.

Principal Component Analysis

Principle component analysis has been described in a number of books and articles and will be discussed here only in general terms.[1,2] The mathematical analyses used in this paper were done using a variant of the Chemometrics Toolbox set of programs developed for use with the MATLAB language.[3] This is a high level language especially designed for solving matrix algebra problems. Some analysis techniques such as varimax rotation, cross

validation and variance ratio F-tests are not included in the Toolbox routines and have been written using the MATLAB language.

The essence of PCA is to extract from the response matrix the important correlations between the various responses. This analysis of the response matrix alone is related to the more complete analysis of the response and factor matrices together using PLS. A PCA analysis may be thought of as a zeroth order PLS analysis, wherein the response or factor matrix is analyzed alone.[4]

The PCA method consists of expanding the response matrix into a sum of uncorrelated matrices, each of which is the outer product of a single score vector(column) and a single transposed loading vector(row). In vector notation, we can write this decomposition

$$\mathbf{Y} = \mathbf{t}_1 * \mathbf{p}_1' + \mathbf{t}_2 * \mathbf{p}_2' + \ldots + \mathbf{E}, \qquad (1)$$

where **Y** is the original response matrix, **t** is a score vector, **p'** is the transposed loading vector, and the matrix **E** contains the residual, i. e. the part of the data not "explained" by the principal components. A primed vector or matrix is a transposed matrix or vector, i. e. $a_{ji}' = a_{ij}$.[5] The loading vectors, **p**, are eigenvectors of the covariance matrix **Y'** * **Y** and the score vectors, **t**, are the eigenvectors of the association matrix **Y** * **Y'**. If the response matrix has N rows(samples) and P columns(responses), **t** is an N x 1 column vector, **p'** is a 1 x P row vector and the outer product **t** * **p'** is an N x P matrix. The orthonormal loading vectors in the response space are a new set of axes that point in the directions of greatest variation and, the P elements of **p'** are the direction cosines to the original response space axes. The N elements of **t** are the coordinates of each of the N sample points with regard to each loading vector axis. If the N points in response space are projected perpendicularly onto a plane defined by two of the loading vectors, the coordinates of the projected points in the plane are the elements of the corresponding score vectors.

The response matrix **Y** presumably contains some noise as well as real variation. If we use all P loading vectors in Eq. (1), we will reproduce the response matrix exactly, noise and all. The object of PCA is to select a smaller number of principal components that will explain almost all of the real variance plus some imbedded error and leave a residual matrix that is almost all noise. This is especially important when P is large. It can be shown that the imbedded noise in the sum of a selected number of eigenvectors is less than the noise included in the sum of all of the eigenvectors.[6] In this way some of the noise can be eliminated from the data. A simple example of this from Reference 6 is shown in Table III. If we construct a simple "pure data" matrix $\mathbf{D}^*$ and add to it a "noise" matrix **N**, we obtain a matrix

containing real variation and noise, **D**. We can easily find the principal components of this matrix using a one line MATLAB language command:

[**load**,**score**,**value**,remvar,modpwr,explvar] = pcarow(**D**), (2)

where **load** is the calculated matrix of loading vectors, **score** is the calculated matrix of score vectors, **value** is the column vector of eigenvalues, remvar is the remaining variance after subtracting the variance explained by the current principle component, modpwr is the modeling power or explained standard deviation per variable, and explvar is a column vector containing the explained variance for each response for each component.[1]

Although in this simple example it is obvious that the two columns in $\mathbf{D}^*$ are not linearly independent, this condition is recognized automatically by the PCA analysis of $\mathbf{D}^*$ and one of the two eigenvalues and corresponding score vectors are zero. Because of the added noise, the columns of matrix **D** are independent and two, non-zero eigenvalues are found: 767.15 and 0.29. It is clear from the size of the eigenvalues that the first outer product, **t1*p1'** will explain almost all of the variation in **D**, and as Table III shows, this matrix reproduces $\mathbf{D}^*$ the "pure data" quite closely. The second matrix factor **t2*p2'** contains mostly noise as can be seen. Of course, the sum of the two factors reproduces **D** exactly. This elimination of the noise rests on the fact that PCA is a least squares procedure and random variations tend to average out.

The value of PCA lies in the fact that in most cases a matrix containing a large number of columns can be approximated quite well by only a few principal components. In the case of the nine column response matrix shown in Table II, only four principal components are needed to explain the important variation. Methods for choosing the proper number of principal components are available.[7]

Since each loading vector can contain contributions from several responses if they are correlated, it may be difficult to relate changes in the principal components to changes in the individual variable values, although in many cases a particular variable is responsible for most of the variation. Although PCA is a least-squares procedure, the number of runs needed to determine the principal components does not need to be large. In the case of the eleven factor nickel process study described above, seventeen sample runs were sufficient. As long as the number of principal components needed to explain most of the variation is less than about a third of the number of samples, the procedure is stable.[8]

Partial Least Squares

The PCA analysis described above will analyze the factor and response matrices separately, but is not able to construct a relation between them. If the two matrices arise from the same underlying model, we can find a relation between them using PLS. This analysis is equivalent to a PCA of each matrix followed by a small rotation of the **X** and **Y** matrices so that the distance between the two matrices represented as points in sample space is a minimum.[9] In this new subspace, in addition to the principal component factorization for each matrix, we can obtain a relation between the matrices by means of a relation between the score vectors of the two matrices. These relations are summarized by the equations:

$$\begin{aligned} \mathbf{X} &= \mathbf{T} * \mathbf{P}' + \mathbf{E}, \\ \mathbf{Y} &= \mathbf{U} * \mathbf{Q}' + \mathbf{F}, \\ \mathbf{U} &= \mathbf{B} * \mathbf{T}, \end{aligned} \qquad (3)$$

where **T** is a matrix of the **X** score vectors, **U** is a matrix of the **Y** score vectors, **P'** is a matrix of the transposed **X** loading vectors, **Q'** is the matrix of the transposed **Y** loading vectors and **B** is a diagonal matrix that connects the score vectors of the two matrices.This last equation is commonly referred to as the inner relation.[10]

If the conditions causing the variation in the two matrices arise from the same cause, we would expect that the loading vectors for both matrices would be parallel and that $\mathbf{t}_i$ and $\mathbf{u}_i$ would differ only in length. A plot of the first two columns of **U** vs. **T** calculated from the data illustrated in Tables I and II are shown in Figs. 1 and 2. The Figures show that the score vectors are indeed parallel and a linear equation of this type fits the experimental data quite well. This means that we can express the Y matrix scores in terms of the X matrix scores with some confidence and that there is a good underlying model that relates the plating factors to the plating responses.[11]

The calculated regression coefficients using the **B** matrix calculated from the data illustrated in Tables I and II are shown in Table IV. The value of PLS modelling is that we can obtain a quantitative model of an electroplating process relating the plating responses to the plating factors even though we do not know the chemical reactions taking place in the bath. In a similar manner we could just as easily have labeled the factor matrix as the Y matrix and response matrix as the X matrix and obtain a "backward" regression matrix relating the plating factors to the plating responses. This would be useful in determining what adjustments to the plating bath parameters should be made to

achieve a desired set of responses.

Process Control

The reduction in the number of components needed to model a multivariate process using PCA or PLS is especially valuable for the design of a process control scheme. The usual method for univariate control is to construct a Shewhart chart, as shown in Figure 3, to monitor the variation of some response between an upper and lower control limit. A multivariate analog of this type of chart can be constructed using the first two or three score vectors that in many cases are all that are necessary to model the important variation in the plating process. If we use the score vector components obtained from a previous set of runs we can construct an area in two dimensional score space or a volume in three dimensional space corresponding to the normal control range of the score components. These two- or three dimensional control limits can then be plotted in an analogous way to those on a Shewhart chart.

Even if some of the process parameters occasionally stray outside the control limits, the model will still be valid and we can still predict the responses, although they will change accordingly. If we compare the predicted and measured responses they should still be close, and the sum of the squares of the differences between the predicted and measured response matrices(PRESS) will be small. On the other hand, if the model ceases to be valid because we have left out an important process parameter which has since changed, or some large change in the nonlinear bath behavior has occurred as a result of a small change in the plating factors; the PRESS will be large even if the process factors are close to their normal range. If we also display the PRESS on the multivariate Shewhart chart we are able to distinguish between these two events.[12] An example of a multivariate Shewhart analogue with two principal components adapted from Reference 12 is shown in Figure 4.

In this way we can distinguish between changes in the process variables and changes in the underlying bath chemistry. We can identify any change in bath chemistry by constructing a new PLS model from the current factors and new responses and comparing this new regression matrix with the old one. Large changes in the coefficients will point to the plating factors that have changed in significance. It may be possible to correct for the new bath behavior by calculating a new "backward" regression matrix as discussed above, and calculating the new values of the bath parameters needed to give the old responses.

The methodology described here is completely general and is not limited to electroplating. These techniques can also be applied to control of a rinse tank system, metal recovery system, etc.

Applications of PLS to control of a fluidized bed reactor and an extractive distillation column are illustrated in Reference 12.

References

1. S. Wold, K. Esbensen and P. Geladi, "Principal component analysis", Chemom. and Intell. Lab. Syst. 2, 37-52(1987).

2. J. Joliffe, Principal Component Analysis, (Springer,Berlin,1986); K. R. Beebe and B. R. Kowalski,"An introduction to multivariate calibration and analysis", Anal. Chem., 59(17),1007A-1017A(1987).

3. MATLAB for MS-DOS Personal Computers, The MathWorks Inc. Natick, MA 01760.

4. P. Geladi, "Notes on the history and nature of partial least squares(PLS) modeling",J. of Chemom., 2, 231(1988).

5. P. G. N. Digby, "Matrix algebra for data analysis", in Food Research and Data Analysis edited by Harald Martens and Hellmut Russwurm(Elsevier, New York, 1983) P. 453-472.

6. E. A. Malinowski, "Theory of Error in Factor Analysis", Anal. Chem. 49(4), 606-612(1977).

7. M. A. Sharaf, D. L. Illman and B. R. Kowalski, Chemometrics, (Wiley,New York,1986)p. 254; E. R. Malinowski, "Statistical F-tests for abstract factor analysis and target testing, J. Chemom. 3, 49-60(1988).

8. S. Wold et al., "Modelling data tables by principal components and PLS: class patterns and quantitative predictive relations", Analusis 12(10), 477-485(1984).

9. A. Höskuldsson, "PLS regression methods", J. Chemom. 2,211-228(1988).

10. H. Martens and T. Næs, Multivarate Calibration(Wiley,New York,1989), p. 116; W. P. P.Geladi and B. R. Kowalski, "Partial least-squares regression: a tutorial", Anal. Chim. Acta, 185,1-17(1986).

11. K. R. Beebe and B. R. Kowalski, loc. cit. p. 1015A.

12. J. V. Kresta et al., "Multivariate Statistical Monitoring of Process Operating Performance", Can. J. Chem. Eng. 69 35-47(1991).

TABLE I

NICKEL PROCESS VARIATION PLATING FACTOR(X) MATRIX

Factor	1	2	3	4	5	6	7	8	9	10	11
Sample	Nickel Conc	Primary Anion	Sec. Anion	Boric Acid	Cu ppm	Fe ppm	Zn ppm	pH	Temp	ASF	Thick
1	-1	-1	-1	-1	-1	-1	-1	-1	-1	-1	-1
2	-1	-1	-1	-1	-1	-1	-1	1	1	1	1
3	-1	-1	-1	1	1	1	1	1	1	-1	-1
4	-1	-1	-1	1	1	1	1	-1	-1	1	1
5	-1	1	1	1	1	-1	-1	-1	1	1	-1
6	-1	1	1	1	1	-1	-1	1	-1	-1	1
7	-1	1	1	-1	-1	1	1	1	-1	1	-1
8	-1	1	1	-1	-1	1	1	-1	1	-1	1
9	1	1	-1	-1	1	1	-1	-1	-1	1	1
10	1	1	-1	-1	1	1	-1	1	1	-1	-1
11	1	1	-1	1	-1	-1	1	1	1	1	1
12	1	1	-1	1	-1	-1	1	-1	-1	-1	-1
13	1	-1	1	1	-1	1	-1	-1	1	-1	1
14	1	-1	1	1	-1	1	-1	1	-1	1	-1
15	1	-1	1	-1	1	-1	1	1	-1	-1	1
16	1	-1	1	-1	1	-1	1	-1	1	1	-1

TABLE II

NICKEL PROCESS VARIATION RESPONSE(Y) MATRIX

Original Data

Sample	R_Stress ksi	I(111)	I(200)	I(220)	I(331)	Duct. %	Rough. microin	P_stress ksi	Con. Res. mohm
1	74.3	0.85	1.84	0.35	0.4	8.37	5.49	16.11	5.30
2	47.4	0.71	2.23	0.25	0.35	9.87	4.36	9.426	5.30
3	-55.5	0.2	0.51	4.56	3.24	3.84	3.38	11.14	1.40
4	37.2	0.6	2.61	0.13	0.23	9.87	4.36	12.854	35.00
5	24.7	0.8	1.25	1.28	1.33	7.12	14.2	6.512	3.80
6	12.2	0.55	2.66	0.18	0.3	4.95	5.56	3.856	12.00
7	18.3	0.51	2.85	0.1	0.15	5.92	3.53	7.284	410.00
8	11.4	1.13	1.15	0.42	0.52	6.58	3.3	4.285	1.24
9	21.1	0.2	3.63	0.04	0.08	6.66	3.76	4.627	35.00
10	6.14	0.85	1.42	0.89	0.96	6.14	5.04	3.428	2.90
11	-9.77	0.55	0.49	3.3	2.71	4.89	4.28	6.427	1.25
12	-6.06	0.38	0.86	3.54	2.39	4.83	3.6	17.995	2.95
13	46.3	0.2	0.99	3.93	2.7	5.58	6.39	11.14	5.30
14	38.3	0.59	2.63	0.06	0.16	7.77	5.94	22.279	9.50
15	22.2	0.82	1.87	0.35	0.53	9.32	12.7	18.851	4.60
16	18.7	0.34	0.6	3.53	3.52	7.77	15.3	11.997	1.50

Centered and Scaled

Sample	R_Stress	I(111)	I(200)	I(220)	I(331)	Duct.	Rough.	P_stress	Con. Res.
1	1.90	0.99	0.12	-0.64	-0.66	0.82	-0.21	0.95	-0.28
2	0.97	0.48	0.53	-0.70	-0.70	1.62	-0.49	-0.19	-0.28
3	-2.57	-1.40	-1.26	1.86	1.63	-1.61	-0.74	0.11	-0.32
4	0.62	0.07	0.92	-0.78	-0.80	1.62	-0.49	0.40	0.01
5	0.19	0.81	-0.49	-0.09	0.09	0.15	1.98	-0.68	-0.29
6	-0.24	-0.11	0.97	-0.75	-0.75	-1.02	-0.19	-1.14	-0.21
7	-0.03	-0.26	1.17	-0.79	-0.87	-0.49	-0.70	-0.55	3.73
8	-0.27	2.02	-0.60	-0.60	-0.57	-0.14	-0.76	-1.06	-0.32
9	0.07	-1.40	1.98	-0.83	-0.92	-0.10	-0.64	-1.00	0.01
10	-0.45	0.99	-0.32	-0.32	-0.21	-0.38	-0.32	-1.21	-0.30
11	-1.00	-0.11	-1.28	1.11	1.20	-1.05	-0.51	-0.70	-0.32
12	-0.87	-0.74	-0.90	1.26	0.94	-1.08	-0.68	1.28	-0.30
13	0.93	-1.40	-0.76	1.49	1.19	-0.68	0.02	0.11	-0.28
14	0.66	0.04	0.94	-0.82	-0.86	0.50	-0.10	2.01	-0.24
15	0.10	0.88	0.15	-0.64	-0.56	1.33	1.60	1.42	-0.29
16	-0.02	-0.88	-1.17	1.25	1.85	0.50	2.25	0.25	-0.32

TABLE III NOISE ELIMINATION USING PRINCIPAL COMPONENT ANALYSIS

Pure Data Matrix D*		Noise Matrix E		Pure Data plus Noise D = D* + E	
1	1	0.2	0	1.2	1
2	2	-0.2	-0.2	1.8	1.8
3	3	-0.1	0.1	2.9	3.1
4	4	0	-0.1	4	3.9
5	5	-0.1	0	4.9	5
6	6	0.2	-0.2	6.2	5.8
7	7	0.2	-0.1	7.2	6.9
8	8	-0.2	0.1	7.8	8.1
9	9	-0.2	0.1	8.8	9.1
10	10	-0.1	0.2	9.9	10.2

First Factor Matrix t1 * p1'		Second Factor Matrix t2 * p2'		Sum of Factor Matrices t1*p1'+t2*p2'	
1.0936	1.1052	0.1064	-0.1052	1.2	1
1.7904	1.8095	0.0096	-0.0095	1.8	1.8
2.9846	3.0163	-0.0846	0.0837	2.9	3.1
3.9288	3.9705	0.0712	-0.0705	4	3.9
4.924	4.9763	-0.0240	0.0237	4.9	5
5.9671	6.0305	0.2329	-0.2305	6.2	5.8
7.0118	7.0862	0.1882	-0.1862	7.2	6.9
7.9086	7.9926	-0.1086	0.1074	7.8	8.1
8.9033	8.9978	-0.1033	0.1022	8.8	9.1
9.9974	10.1036	-0.0974	0.0964	9.9	10.2

TABLE IV

ONE FACTOR INTERACTION REGRESSION COEFFICIENTS

Response	Ni x1	Prim. Anion x2	Sec. Anion x3	Boric Acid x4	Cu Imp. x5	Fe Imp. x6
R-Stress	-0.0231	-0.0877	0.0205	-0.0780	-0.0599	-0.0194
I(111)	-0.0796	0.0342	0.0234	-0.0840	-0.0261	-0.0335
I(200)	-0.0456	0.0086	0.0076	-0.0639	0.0261	0.0551
I(220)	0.0809	-0.0247	-0.0239	0.1014	-0.0117	-0.0219
I(331)	0.0799	-0.0247	-0.0091	0.0919	0.0011	-0.0375
Duct.	-0.0121	-0.0916	0.0266	-0.0643	-0.0027	-0.0378
Rough.	0.0376	-0.0606	0.0884	-0.0210	0.0744	-0.0970
P-Stress	0.0627	-0.1546	0.0005	0.0386	-0.0367	-0.0223
Con.Res.	-0.0520	0.0594	0.0601	-0.0503	-0.0420	0.0564

	Zn Imp. x7	pH x8	Temp. x9	Curr. Dens. x10	Thick. x11
R-Stress	-0.1066	-0.0711	-0.0615	0.0618	0.0481
I(111)	-0.0127	0.0194	0.0112	-0.0353	0.0202
I(200)	-0.0876	0.0232	-0.1519	0.0808	0.0600
I(220)	0.0800	-0.0278	0.1160	-0.0489	-0.0601
I(331)	0.0769	-0.0341	0.1289	-0.0446	-0.0603
Duct.	-0.0775	-0.0358	-0.0815	0.0438	0.0366
Rough.	0.0071	-0.0413	0.0440	0.0344	-0.0320
P-Stress	0.0437	0.0000	-0.1049	0.0012	-0.0574
Con.Res.	0.0373	0.0478	-0.0762	0.0584	-0.0454

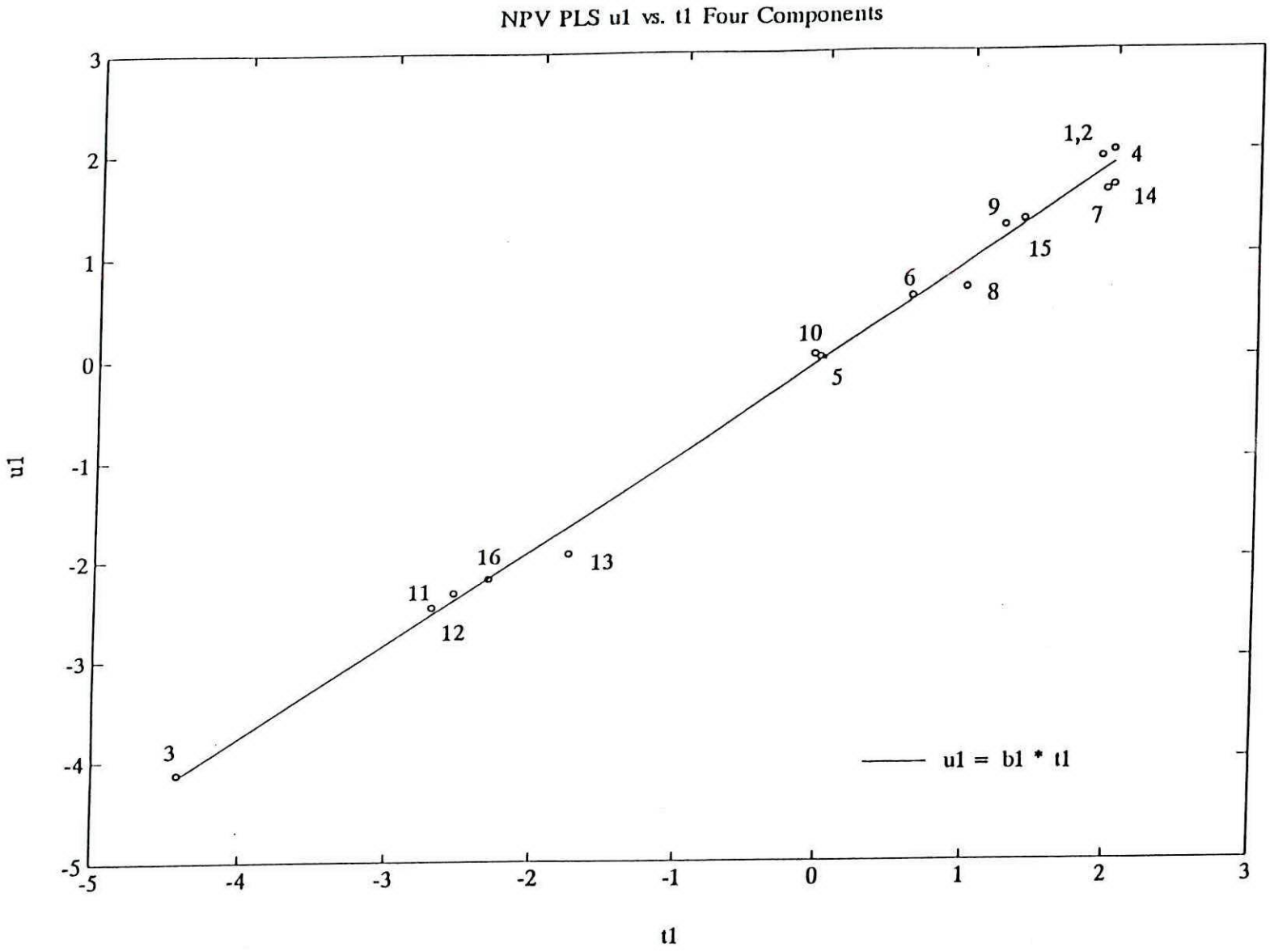

FIG. 1. Score plot for the first Y matrix score coefficients u1 vs. the X matrix score coefficients t1. The straight line is the inner relation, u1 = b1 * t1.

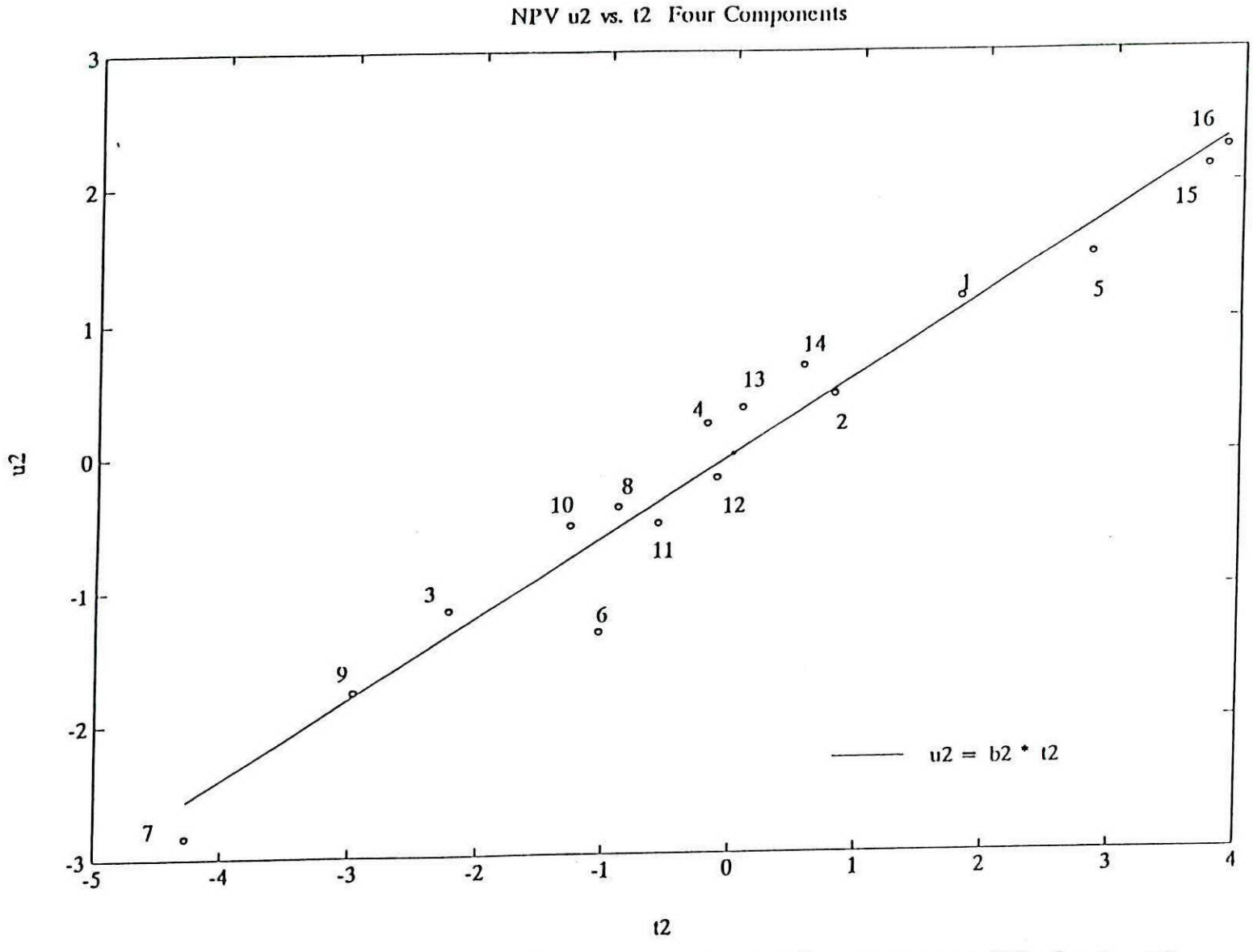

FIG. 2. Score plot for the second Y matrix score coefficients u2 vs. the X matrix score coefficients t2. The straight line is the inner relation, u2 = b2 * t2.

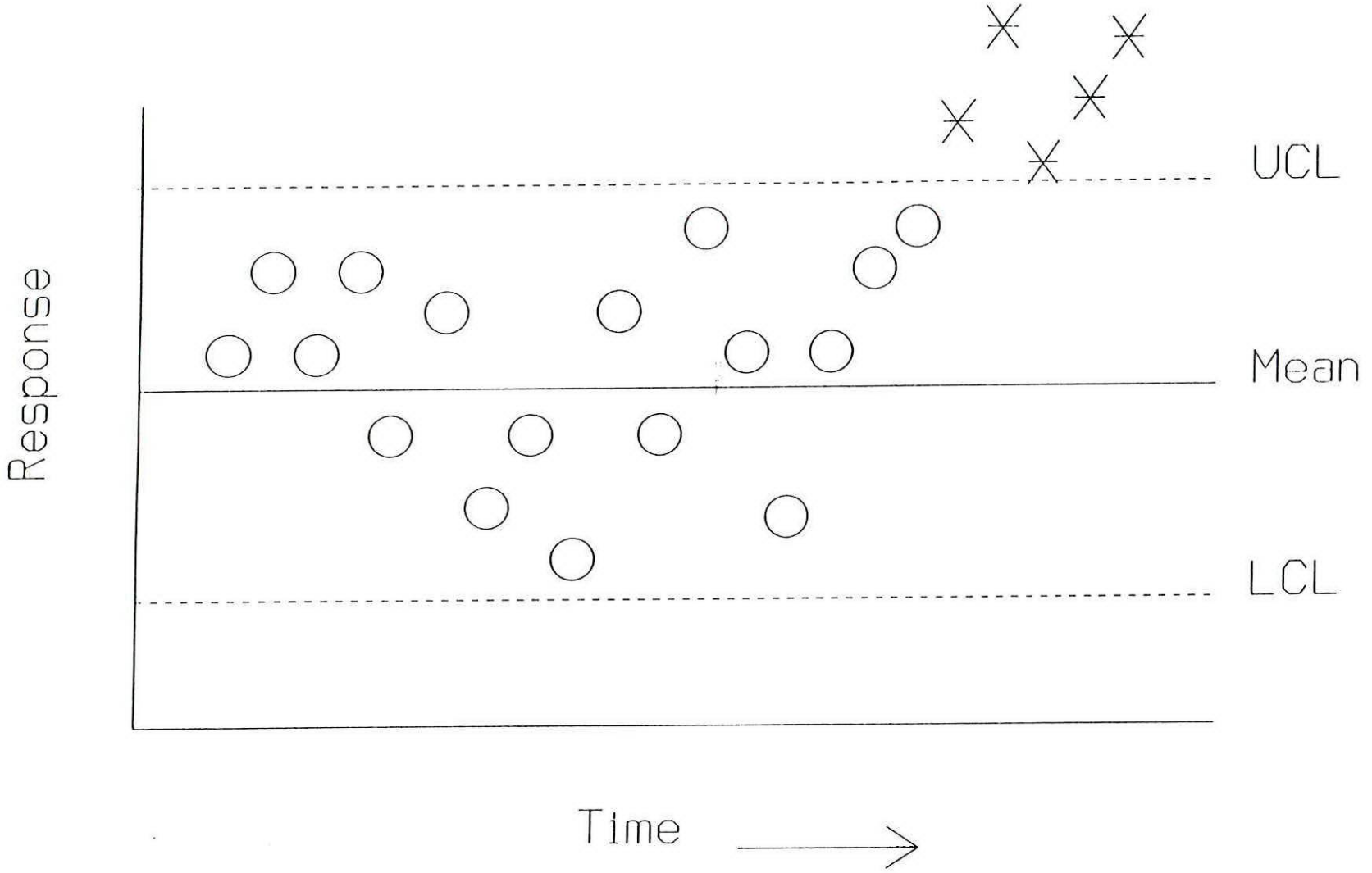

FIG. 3. A univariate Shewhart chart. The responses within the upper and lower control limits (o) are in control, and those outside these limits (*) are out of control.

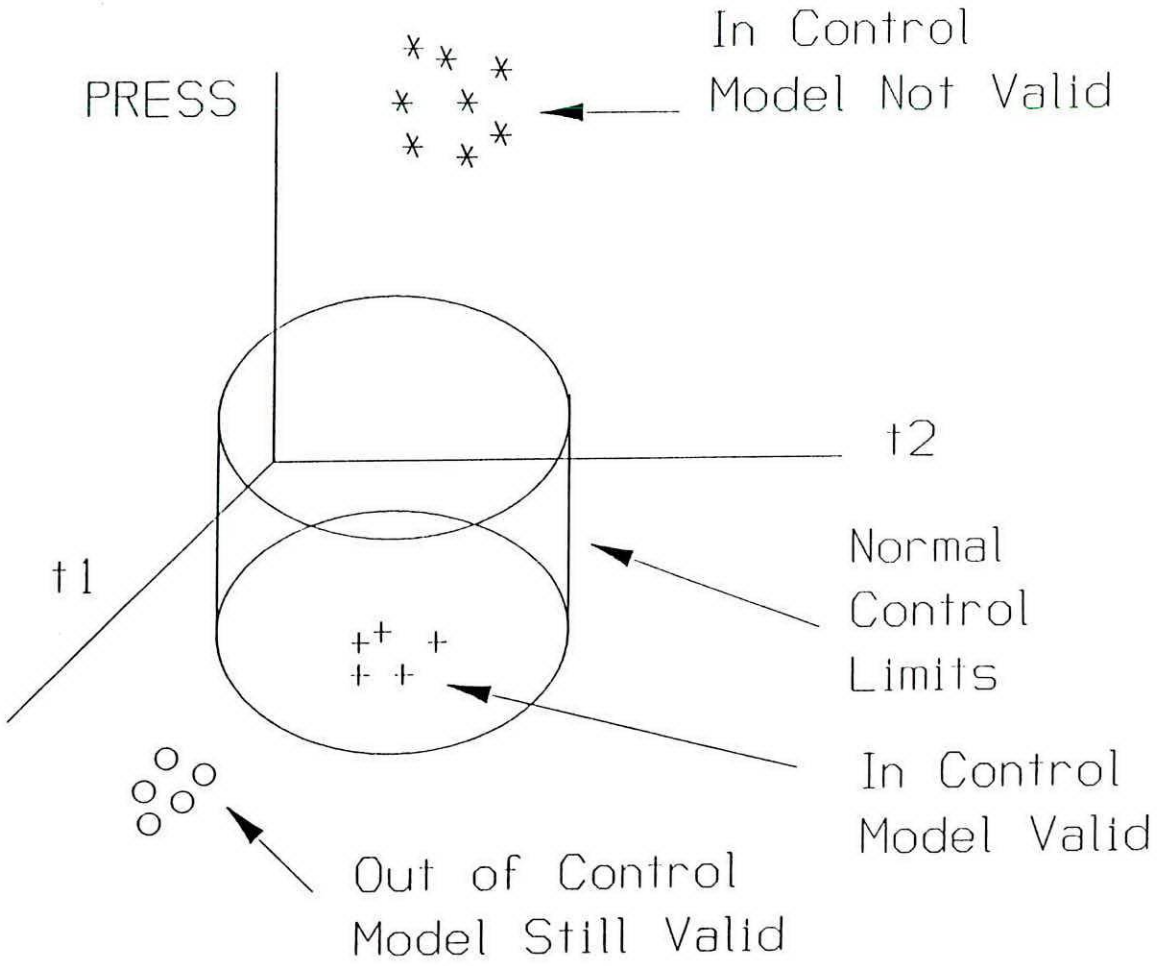

FIG. 4. A multivarate analog of a Shewhart chart for a process with two latent variables. The orthogonal axes are the two corresponding score vectors (t1 and t2) and the squared difference between the predicted and measured response matrix (PRESS). The data points illustrate: (+), a process in control with a valid regression model; (o), a process out of control with the same valid model; and (*), a process with bath parameters within the normal operating limits but with an invalid regression model.

Advanced Surface Finishing Technology for Electronics Application

Tetsuya Osaka

Department of Applied Chemistry, Waseda University
Okubo, Shinjuku-ku, Tokyo 169, Japan

The surface finishing technology used in advanced electronics field is reviewed. In particular, topics in the areas of printed wiring boards, hybrid IC, and magnetic recording fields will be discussed.

Printed Wiring Board Field

Electroplating and electroless-plating methods are widely used in the electronics application. Table 1 shows some classification of surface finishing technology in electronics. In the field of printed wiring boards (PWB), total market in Japan becomes 1,030 billion yen (8.2 billion US$) in 1990 and will be 1,500 billion yen (12 billion US$) in 1995. In order to increase the packing density, the PWB reaches both techniques to use higher multi-layer and higher surface density. Thus, solder-bonding technology, which cannot decrease the pin hole pitch less than 1.7 mm, changes to surface mounting technology (SMT) system, which can decreases pin hole pitch to 0.3 mm. Such a precise scale for SMT becomes to place a plating technique as one of the key technology. Electroless copper plating for conductors is widely used in the case of through-hole plating, and recently not only the subtractive method but also additive one is gradually increasing for high density PWBs. Direct plating at through-hole instead of electroless copper plating is also proposed. For example, as is shown in Fig. 1, the highest multi-layer ceramic substrate (MLS) board for high speed computer NEC ACOS SYSTEM 3800 consists of three levels[1]; the first level is tape automated bonding (TAB) LSI and its flipped TAB carrier (FTC), the second level is MCP mounted on MLS and its liquid cooling module (LCM), and the third level is the high multi-layer PWB mounted the second level LSI ultra high density packaging multi-chip package (MCP). The second level MLS is more than 40 multi-layer ceramic board and polyimide multi-layer, and the total becomes almost 70 layers as is shown in Fig.2. In the MLS, the gold plating is used for 75 μm pitch with 25 μm width.

Fig.1 Packaging hierarchy for NEC ACOS 3800 computer system.

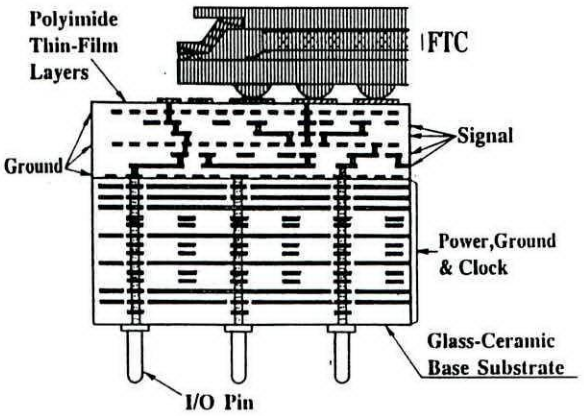

Fig.2 Multilayer PWB using ceramic and polyimide boards (70 layers) for NEC ACOS 3800 computer system.

Hybrid IC and Thin Film Resistors

As is shown in Table 1, plating films are also used for connectors, electrode connectors, resistors, and EMI shielding. Electroless nickel film is extensively used in this field. For the thin film resistor, NiWP and NiCrP films are attempted for higher stability resistor film than an amorphous NiP one against heat shock atmosphere. Figure 3 is an example of thin film resistor for thermal head printer, which is composed of electroless NiWP film with higher thermal stability.[2] A nickel alloy system can be used for an effective method of improving thermal stability of plating film. Figure 4 demonstrates the stability of nickel alloy films, where three films of NiWP, NiMoP and NiReP works stably until around 500°C as compared with the amorphous NiP being stable until around 300°C.[3]

Magnetic Recording Media Fields

In the field of magnetic recording devices, an electroless CoNiP film is used for high density magnetic recording medium. An electroless plating has an advantage to form homogeneously thin film on the substrate, and its advantage made it practical for use on the 8 inch magnetic rigid disk of the PATTY head disk assembly (HDA) shown in Fig.5 by NTT company in 1981.[4] At that time, the PATTY has 400 MB capacity with 8 disks for one HDA (14 kBPI, 1.1 kTPI), and the total capacity composed of 8 HDA was 3.2 GB, which was the highest magnetic recording density in the world.
In the plated rigid disk, the NEC corporation has continuously de-

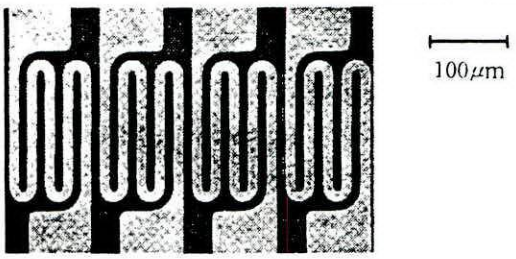

Fig.3 Thin film resistor for thermal head printer made by electroless NiWP.

Table 1 Application of platings to electronic materials.

Printed Writing Boards (PWB)	PWC:	conductor	:Cu
		bonding	:Sn,Ni,Au
		contact	:Ag,Au
	Hybrid IC:	resistors	:Ni
		conductor	:Cu,Ag,Au
Magnetic Recording Materials	Magnetic disk:	memory medium	:Co,CoNi
		underlayer	:NiP
	Magnetic Tape:	memory medium	:Co,CoNi
	Magnetic head:	soft magnetics	:NiFe
Contact Materials	Connector	:Ni,Ag,Au	
	Bump	:Ni,Ag,Au	
High Frequency Materials	Micro wave conductor	:Cu,Ni,Ag,Au	
Si Semiconductor Devices	Solar cell connector	:Ni	
	Si device interconnector	:Ni,Cu	
GaAs Semiconductor Devices	Ohmic contact electrode	:Ni	
Display Devices	LCD electrode	:Ni	
Electromagnetic Interference (EMI)	Conductor and anticorrosion	:Cu,Ni	

veloped higher level HDA, i.e., 520 MB, 800 MB, 1.1GB, 1.4 GB, 3GB per HDA.[5] In the 3GB HDA, the linear density and the track density becomes 38 kBPI and 1.7 kTPI, respectively. In the rigid disk process, the electroless NiP film with amorphous state is used for the underlayer plated on aluminum alloy substrate. For future higher density magnetic recording system, the perpendicular magnetic recording media are developed by electroless CoNiReP and CoNiP films. Figure 6 shows representative properties of the CoNiReP media. Such media demonstrate so high recording density D_{50}= 172 kFRPI[6] and 134 kFRPI[7] for CoNiReP/NiWP floppy disk and CoNiReP/NiFeP rigid disk, respectively, with a combination of ring-type head.

Magnetic Head Field

In the case of the thin film head shown in Fig. 7, core material of permalloy (NiFe) is plated by electrodeposition with frame plating method. In this process, the composition of permalloy must be controlled so rigidly within 0.1 wt%, and the paddle agitation which produces a laminar flow in the plating bath, depresses the composition inhomogeneity to control the difference of metal ion concentrations at the interface and bulk regions. The frame plating method is also used to avoid the inhomogeneity of current density distribution at the precise area.[8] The coil pattern for the thin film head is formed by Cu plating, where the coil width is 3.5 μm with 3 μm pitch.[9] For future soft magnetic materials possessing higher saturation magnetic flux density, Bs, we are developing the electroless-plated CoB and CoFeB films, whose Bss' are 1.45 T; ca. 1.5 times large than NiFe permalloy film.[10] Figure 8 shows representative properties of the CoB films.

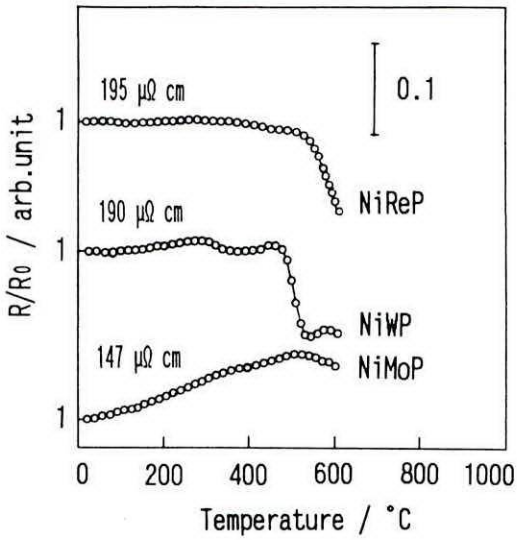

Fig.4 Change in specific resistance of electroless NiReP (annealed at 500°C, 1hr), NiWP (annealed at 400°C, 1hr), and NiMoP (annealed at 500°C, 1hr) films during heat treatment.

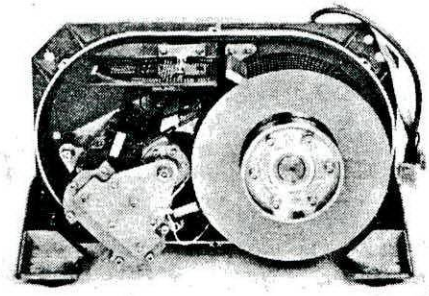

Fig.5 PATTY Head Disk Assembly using plated disks [400MB/HDA] by NTT at 1981.

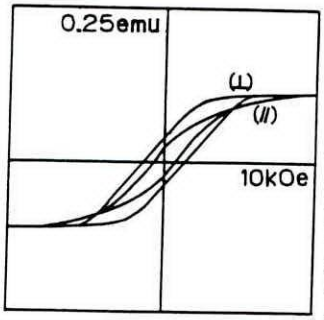

$Co_{32}Ni_{55}Re_6P_7$ at%
Ms 250 emu/cc
Hc(⊥) 1200 Oe
Hc(//) 600 Oe

Fig.6 Representative magnetic properties of electroless CoNiReP perpendicular magnetic recording medium.

Optical Disk Field

For optical-disk field, the stampers for ROM and erasable CDs are formed by a Ni plating on sputtered Ni on glass substrate. In these disks, groove and signal are memorized within 1.6 μm pitch track width, and in the erasable photo disk, tracing groove, sector mark and address mark are also registered within 1.6 μm pitch track width.[11)]

EMI Shielding Field

Recently, demand of shielding for electronic devices is requested for protection of miss-controlling the computer devices. An electroless Cu and Ni plating on housing of devices are interested in, and the housing of lap-top personal computer made by polycarbonate plastics is plated by the electroless Cu film with 1 μm and after Ni with 0.25 μm for EMI shielding.[12)]

Conclusion

Advanced surface finishing technology in electronics application is described. In this field, the plating technique has become an important key technology. In the future there will be an increase usage of more advanced plating developed technique and also for the field of using the advantages of plating techniques.

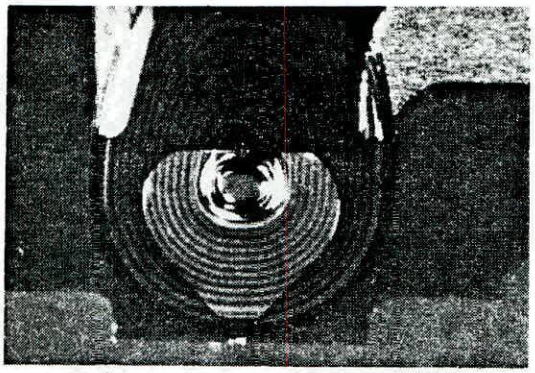

Fig.7 Thin film head made by NiFe plating for core and Co plating for coil.

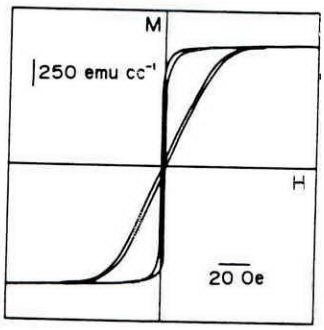

$Co_{96}B_4$ at%	
Bs	1.45T
Hc	0.64 Oe
μ	>2000*

* by annealing at 150°C with applying an external field.

Fig.8 Representative magnetic properties of electroless CoB soft magnetic film.

References

1. Y.Shimada,A.Dohya,K.Kata,J.Inasaka, Proc. of 1991 Int.Symp. on Microelectronics, p.176 (1991.10).
2. H.Sawai and T.Osaka, J.Surf.Finishing Soc. Jpn., 42, 888 (1991).
3. T.Osaka,M.Fukawa and S.Ueda, Proc. Interfinish'92, 1240(1992).
4. S.Hattori,A.Tago,Y.Ishii,A.Terada, O.Ishii and S.Ohta, Elec.Comm.Lab. Tech.J.,31, 277 (1982).
5. F.Goto, "High-functionally Thin Film Formation Methods Using Wet Process,"T.Osaka and K.Nihei,Eds., p.23, Koshinsya, Tokyo (1991).
6. H.Matsubara, S.Mitamura, K.Noda, T.Osaka and F.Goto, J.Magn.Soc. Jpn., 13, 153 (1989).
7. T.Osaka,T.Homma,K.Saito,K.Noda, F. Goto,N.Shiota and T.Yamamoto,IECEJ Tech.Rep., MR90-10, 1 (1990).
8. D.A.Thompson and L.T.Romankiw, IBM Disk Storage Tech.,3 (1980).
9. K.Ohashi, M.Ito and M.Watanabe, Proc. Vol.88-23, p.525, Electrochem. Soc, Pennington (1988).
10. T.Osaka, T.Homma, K.Saito, A.Takekoshi,Y.Yamazaki and T.Namikawa,J. Electrochem.Soc., 139,1311 (1992).
11. N.Imamura, J.Magn.Soc.Jpn., 8, 345 (1984).
12. H.Nakao, "High-functionally Thin Film Formation Methods Using Wet Process,"T.Osaka and K.Nihei,Eds., p.297, Koshinsya, Tokyo (1991).

Anodic Oxide Films on Aluminum - Structure and New Applications

by **Nobuyoshi BABA**

Faculty of Technology, Tokyo Metropolitan University
Tokyo, Japan

INTRODUCTION

Porous type anodic oxide film on aluminum is a unique material for its microporous structure. Isolated micropore array is open perpendicicular to the oxide surface, and the size and number of the micropores can be controlled by a electrolysis conditions.

The porous oxide film can be used as a supporting material for separation membranes, sensors and other free-standing materials. By replacing the porous alumina by other materials such as metals, semi-conductors or plastics, a wide variety of new applications is possible.

STRUCTURE of POROUS ANODIC OXIDE FILM on ALUMINUM

Anodic oxide film on aluminum formed in oxalic acid electrolyte shows typical porous structure **(Photo 1)** and the pore diameters can be controlled by immersion dissolution of the pore wall with acid. This technique is well-known as the pore widening method. By this technique a large pore size oxide film can be obtained for the purpose of production of "multicolor anodizing aluminum" [1]) or "magnetic recording media " [2]).

On the other hand, the smaller pore size anodizing alumina film can be obtained by impregnation of colloidal substances in the pore. The CVD method [3,4]) or chemical conversion method [5]) has been reported.

It was however very difficult to impregnate the materials into micropores deeply and uniformly. In most cases the impregnating materials remained only near the opening of the pores.

MICROFABRICATION of POROUS STRUCTURE[6,7])

The structure of porous alumina film is very suitable for the separation membrane or functional electrode because the pore size and the number of pores can be controlled precisely. However the anodized alumina is easily corroded by both acids and bases. Therefore we tried to transfer the microporous structure of anodized alumina films to the other materials, such as metals, semiconductors and polymers. This method is known as the template method.

Figure 1 shows the schematic procedure of several template methods. We can duplicate the microporous structure of anodized alumina film by [1] electrodeposition of metals, [2] electroless metal deposition, [3] sol-gel impregnation method, and [4] sputtering process.

PHOTOGRAPH 2 shows the SEM image of the microporous structure of negative type Ni needles produced by electroless metal deposition. It is clearly seen that nickel columns have grown perpendicular to the substrate metal surface. This shape corresponds to the negative structure of the porous anodic oxide film.

Electrodeposition of precious metals on the negative type nickel columns show again the positive type porous structure of precious metals. After this manner the porous structure of Au can easily be obtained (Photo 3).

The porous metal surface impregnated with glucose oxidase enzyme is electrochemically active to the reduction of molecular oxygen dissolved in water, so that it is applicable to the glucose sensor.

Figure 2 shows the process of microfabrication of porous silicone film on anodized alumina surface. Silicone is Ar - ion sputtered on anodized alumina film and then the anodized alumina film is removed by NaOH solution. The porous structure of the anodized alumina surface is fairly good when reproduced on the sputtered silicone surface as is shown in **Photo 4.**

Figure 5 shows the SEM image of the porous structure of polymer film fabricated by the 2 step template method. Very fine and parallel array structure is clearly observed. In this experiment, methyl-m-acrylate (MMA) and epoxyresine were investigated.

FUTURE APPLICATIONS

The porous structure of duplicated thin film can be used for

1] Semi-transparent electrode for the photo-electrochemical measurements.

2] Selective ion separation membrane [8])

3] Supporting electrode of enzymes or liquid crystals [9])

4] Separation membrane of microbaials or macromolecular substances.

5] Composite film of microporous structure has possibility of multi-functional devices.

LITERATURE

1) K. Wada, K. Uchida; Advanced Metal Finishing Technology in Japan 93(1980) (Technocrat)

2) S. Kawai et al; J. Electrochem.Soc., 122, Vol. 32, 1026(1975), Vol. 123, 1047(1976)

3) K. Arai, H.W. Kang, K. Ishiyama; J. Surface Finishing Soc. Jpn., 42, No. 3,291(1991)

4) H. Masuda and N. Baba; J. Surface Finishing Soc. Jpn., 43,No.2, 42,No. 3,291(1991)

5) S. Ono, Kenji. Wada, T. Yoshino, Kazuhiro. Wada N. Baba; J. Surface Finishing Soc. Jpn, 40, No.9,1039(1989)

6) H. Masuda, H. Tanaka and N. Baba: Chem. Lett. 1990, 621(1990)

7) H.Masuda and N. Baba; J. Surface finishing Soc.Jpn. 41, No.8 813(1990)

8) K. Kuroda; J. Surface Finishing Soc.,Jpn. 40, No.5, 685(1989)

9) S. Morisaki, M. Yamamuro and N. Baba; J. Surface Finishing Soc. Jpn. 40, No. 1,152(1989)

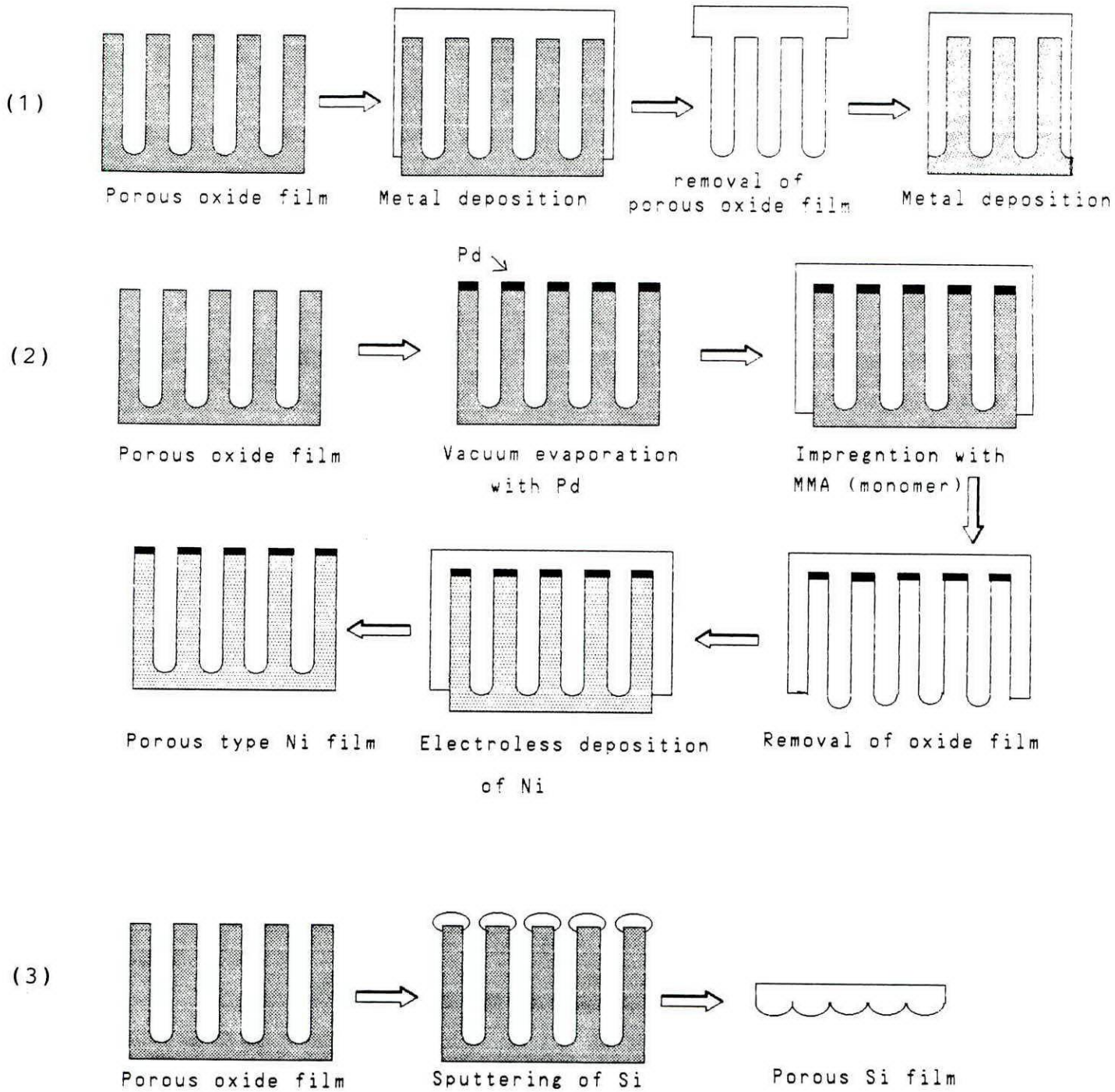

Fig.1 Schematic Procedures of Template Method

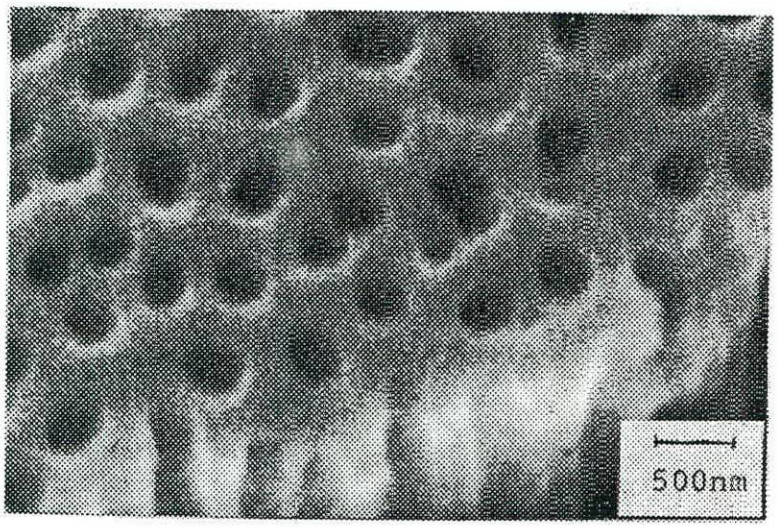

Photo.1 Typical Porous Structure of Anodic Oxide Film on Al formed in Oxalic Acid Electrolyte

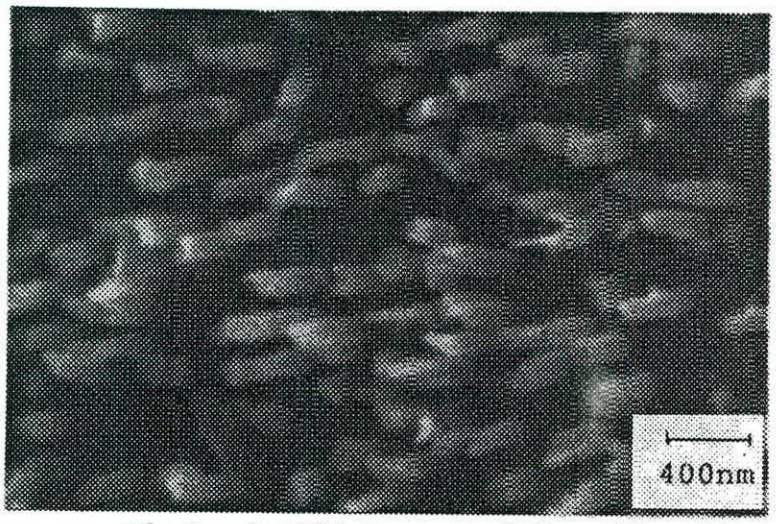

Photo.2 SEM Image of Negative Type Ni Deposit

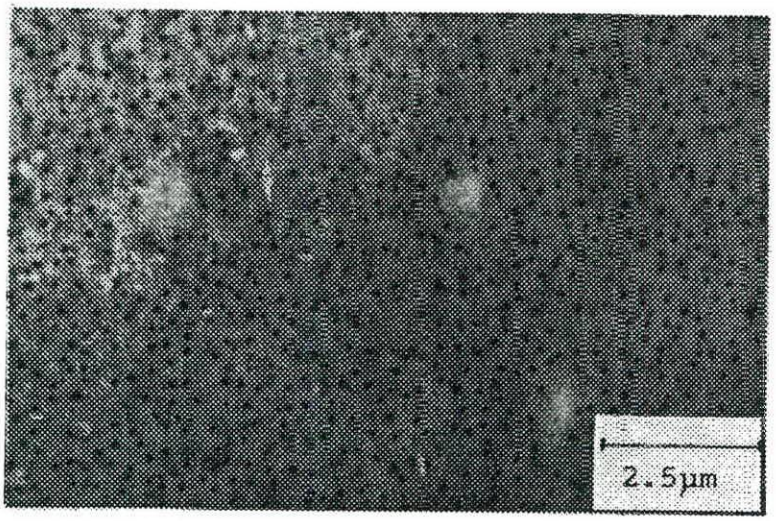

Photo.3 SEM Image of Positive Type Au Deposit

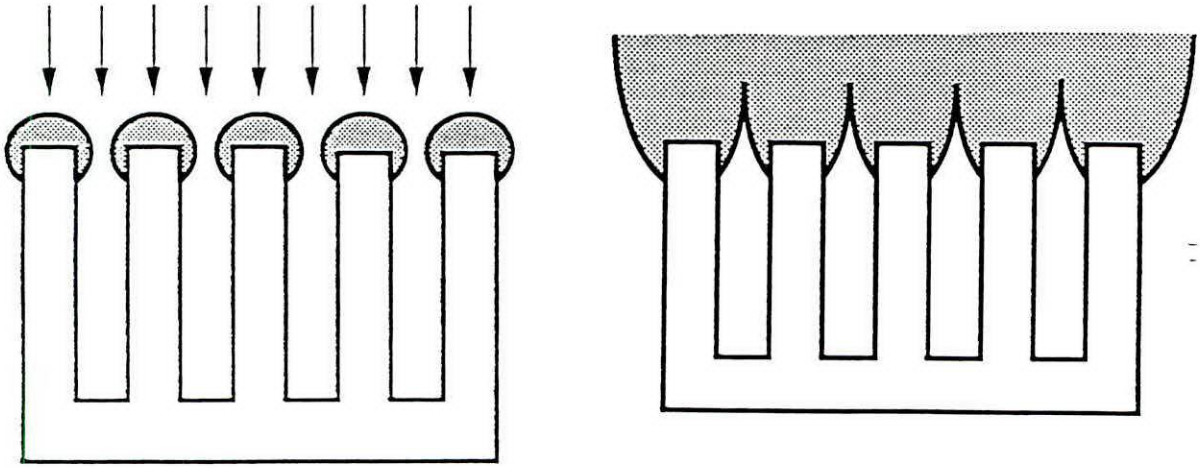

Fig.2 Microfabrication Process of Porous Si Thin Film

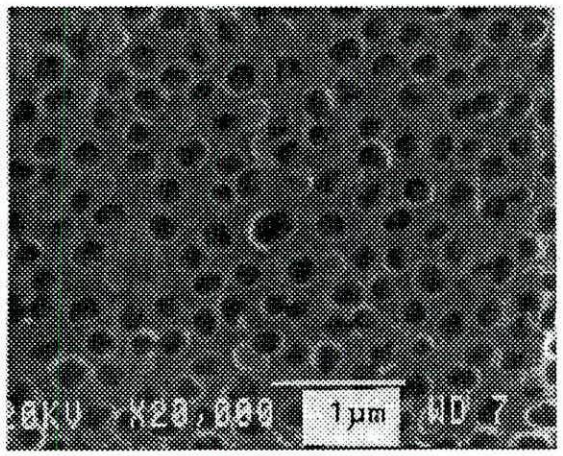

Photo.4 SEM Image of Porous Si Thin Film

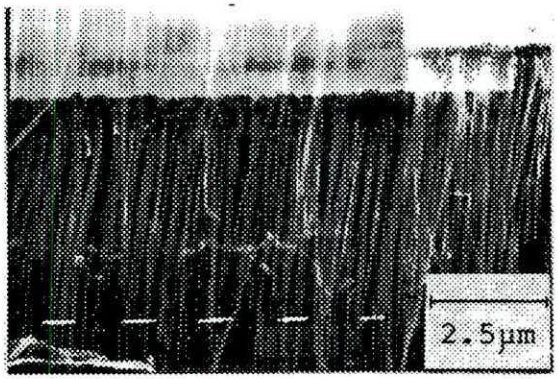

Photo.5 Sectional SEM Image of Porous PMMA Thin Film

ENVIRONMENTAL EFFECTS ON ELECTRONIC MATERIALS

B.I. RICKETT AND J.H. PAYER
Department of Materials Science and Engineering
The Case School of Engineering
Case Western Reserve University
Cleveland, Ohio

With the incorporation of electronic materials and devices into every facet of modern technology, the reliability of a component within its service environment has become a major issue. Environmental attack can originate from a variety of sources, including the action of ambient relative humidity on processing contaminants, the corrosive action of gaseous pollutants, and the deposition of particulates from the atmosphere. A multitude of environmental and material parameters control the aggressiveness and rate of this degradation; thus, a significant amount of research effort has been focused on understanding the mechanisms controlling the overall process. Further research is necessary in order to accomplish the long range goals of predicting component lifetimes, creating accurate accelerated tests, and designing methods to mitigate the environmental effects on materials.

INTRODUCTION

Ensuring the reliability of electronic materials has become an essential product design parameter. Device failure can elicit a variety of reactions from the mild irritation associated with an unreliable hand held calculator to the immense aggravation and high economic costs associated with malfunctioning process control equipment or to the life-threatening possibilities of a faulty automobile air-bag system. One important factor which determines product reliability is the debilitating action of the service environment on electronic components. With the integration of microelectronics into every aspect of modern life, (ie. automobiles, paper mills and processing plants, telecommunications, etc.) the service environment for electronic materials has shifted from benign, atmospherically controlled locales to highly aggressive environments experiencing higher temperatures, relative humidities, and concentrations of particulate and gaseous corrodants. The service conditions encountered by automotive electronics are typical of these new hostile environments: readily available corrosive species from multiple sources, temperature variations between -40 and 150°C, and severe mechanical vibration.[1]

In recognition of the need for product reliability under these strenuous service conditions, many manufacturers have instituted accelerated testing programs for their components; yet, to locate, understand, and predict environmental attack remains a difficult undertaking. This paper will serve to outline some of these important issues, including: the sources of environmental attack, the phenomenology of failure, the controlling environmental parameters, the prediction of component lifetimes, and the methods to prevent environmental attack.

SOURCES OF ENVIRONMENTAL ATTACK

The environmental degradation of electronic materials, in particular metallic conduction pathways and interconnects, often proceeds by means of an electrochemical process. As this is the case, a corrosive electrolyte is required in order to support the oxidation of the underlying metallic substrate and the formation of corrosion product layer, frequently referred to as a "tarnish" film. Water from the environment, as reflected by the surrounding relative humidity, is readily available for adsorption on the surface. This water layer becomes corrosive through the incorporation of various ionic species, which are available from three principal sources: contaminants from processing or handling, atmospheric pollutant gases, and particulate deposition from the atmosphere. Direct precipitation will not be treated as a potential source of corrosive agents for materials utilized in electronics; although, for the recovery of systems which have experienced disastrous conditions, such as fire or flood, this can certainly be an important consideration.

The first source to be considered arises from improper or insufficient cleaning procedures following a processing step or handling either by the manufacturer or the end-user. As an example, military radio components utilized in Vietnam failed when chloride containing flux residues combined with the high humidities of the jungle to destroy the Fe-Ni-

Co leads of transistors.[2] In general, processing steps such as the chemical cleaning of drilled through-holes or immersion in electroless plating baths can introduce surface contaminants which, when exposed to a humid service environment, can lead to the formation of a thin corrosive electrolyte film. The ionic species necessary to support the attack of electronic materials can even arise directly from the constituents of the packaging layers, as exemplified by the potential release of acetic acid from RTV silicone encapsulants.[3]

The presence in the atmosphere of gases, such as SO_2, H_2S, HCl, CO_2, NO_2, NH_3, and O_3, provides a second source of corrosive species. Even at low part per billion concentrations, these gases can dissolve in the thin moisture film on the surface and support electrochemical reactions. Atmospheric compositions and concentrations will depend greatly upon the local environment.[4-9] The indoor levels of most gaseous species are attenuated relative to their outdoor concentrations; however, exceptions such as higher indoor concentrations of NH_3 and HCHO can arise from cleaning solvents, smoking, and other indoor sources.[4]

Variability in pollutant gas concentrations from one urban area to the next prevent the assignment of "typical" values. In the case of sulfur dioxide, levels are reported to range from 5 to 24 ppb.[9] Similarly, urban areas can be characterized by relatively high concentrations for some pollutants and much lower concentrations for others. For a site in Los Angeles, D.W. Rice *et al.* measured higher concentrations of nitrogen dioxide and lower concentrations of reduced sulfur gases than were detected at a site in South Carolina. Furthermore, these same measurements indicated great seasonal fluctuations among individual gaseous species (1.01 $\mu g/m^3$ in the summer versus 10.8 $\mu g/m^3$ in the winter for reduced sulfur gases at the site in South Carolina).[7]

A third source of corrodants arises with the deposition of atmospheric particulates on free surfaces.[7,9-11] These ionic species frequently consist of fine ammonium sulfate particles as small as 0.1 μm in diameter and coarse, calcium-rich particles up to 15 μm in diameter.[10] Particulates can also contain species such as CaO, Al_2O_3, NO_3^-, Cl^-, SiO_2, and alkanes.[9] Apart from providing ionic species for the corrosive electrolyte, these deposited particulates may serve to increase the amount of water, and therefore corrosivity, by presenting a greater surface area for water adsorption and by exhibiting hygroscopic characteristics. Similar to the situation for pollutant gas sources, particulate compositions and fluxes depend upon the location and season for both indoor and outdoor measurements.[7,11]

The incorporation of ionic species from any or all of these sources into the adsorbed water film produces a corrosive electrolyte capable of rendering passive metal oxide layers ineffective and of encouraging the formation of corrosion products. The parameters which control the severity of this environmental attack shall be dealt with later in greater detail.

FAILURE MODES

With the creation of a thin corrosive electrolyte film, electronic conduction pathways and interconnects can fail by several modes, including: electrical shorts through corrosion product bridging, electrical opens due to excessive material loss, and electrical losses between mating connectors. A schematic of these various situations can be seen below in Figure 1.

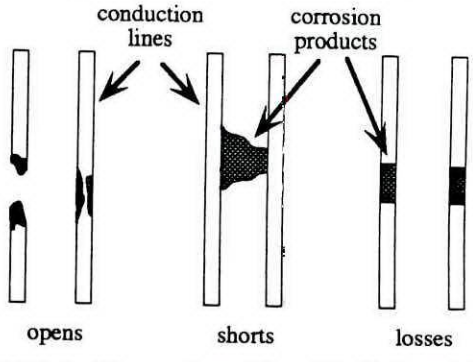

***FIGURE 1:* Illustration of Possible Failure Modes**

The continual drive to miniaturize microcircuitry has led to closely spaced, thin conduction lines which are incapable of tolerating even small amounts of material loss to corrosion. The closer spacing of these lines has also dramatically increased the electric fields which encourage corrosion product bridging. Hence, as the technology behind electronic materials advances, an understanding of the role played by environmental stresses will become even more essential.

PARAMETERS CONTROLLING ENVIRONMENTAL ATTACK

Several parameters control the rate and mode

of environmental attack. Within this paper, these important issues have been grouped in a manner consistent with the natural structure of the environment / substrate system. This organization is illustrated by Figure 2.

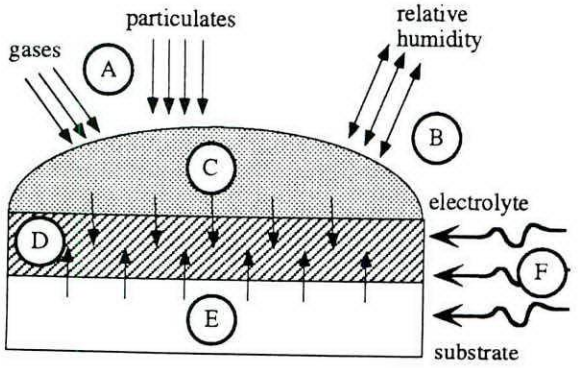

FIGURE 2: **The Various Parameters Controlling the Rate and Mode of Environmental Attack on Electronic Materials**

The parameters of importance are as follows: **A)** mass transport of pollutant gases and particulates, **B)** surface adsorption of water vapor, **C)** physical chemistry of the electrolyte, **D)** film growth processes, **E)** the metallurgy of the underlying substrate, and **F)** the external stresses, such as mechanical, thermal, electrical field, and galvanic factors.

MASS TRANSPORT OF POLLUTANT GASES AND PARTICULATES

One parameter influencing the severity of an environmental attack is the availability of the ionic species necessary for the creation of a corrosive electrolyte. For situations involving contamination from processing or handling, the amount of a particular compound present, such as a chloride, depends upon the amount originally deposited on the surface and the effectiveness of the techniques used subsequently for cleaning. In the case of gaseous or particulate pollutants, the species must first be transported through the gas phase of the service environment to the thin, adsorbed moisture layer on the substrate surface. A tortuous air flow past other susceptible materials can produce a "scavenging" effect which significantly reduces the availability of corrosive species for the substrate of interest. L. Volpe and P.J. Peterson demonstrated that the tarnishing rate of silver exposed to a humidified gas mixture containing 40 ppb (parts per billion) hydrogen sulfide was controlled entirely by gas phase transport, even at their high experimental flow rates.[12] A similar transport limitation arises during the accumulation of particles on a surface. J.D. Sinclair estimated the indoor deposition rate of fine sulfate particles based upon the availability of species outdoors. A 20 $\mu g/m^3$ concentration outdoors could produce a sulfate particle deposition of 0.76 $\mu g/cm^2$ yr indoors.[13] These fine particles, which weigh a fraction of a picogram, are not greatly attenuated from outdoor levels, unlike the coarse particulates which are readily filtered from the air.[13]

Kinetic restrictions are also placed upon the rate of dissolution of these corrosive species into the electrolyte and the rate of transport through the electrolyte to the metallic substrate for reaction. Protective layers, such as gold or polymeric coatings, can serve to limit the transport of the pollutant species, the atmospheric humidity, or both to the surface of the electronic materials, thus impeding the corrosion reaction. Yet, complete separation of a susceptible material from surrounding corrodants is impossible. Moisture can still permeate through most polymeric films, although at a restricted rate, and coatings frequently have defects which provide localized pathways for attack.

SURFACE ADSORPTION OF WATER VAPOR

As asserted for the pollutant gases and particulates, access of water vapor to the surface of an electronic device is an essential parameter in the overall process of environmental attack. The amount of water vapor present on the surface of a material is a function of the relative humidity of the surrounding environment. Likewise, tarnishing rates have been shown to depend very strongly on humidity. Figure 3 displays the influence exerted by relative humidity as determined by D.W. Rice *et.al.*.[6,14] Obviously, wet-dry cycling will dramatically affect the rate of atmospheric attack.

The amount of moisture adsorbed is partially determined by the composition of the surface. Metal oxide layers will adsorb a different amount of water than the pure, unoxidized metal substrate. S.P. Sharma found by quartz crystal measurement techniques that Cu_2O adsorbs approximately twice as much water at 80% relative humidity as metallic Cu.[15] Furthermore, the formation of tarnish film products or the presence of hygroscopic particulates can encourage the adsorption of more water than would

be otherwise present on the surface. Alumina substrates contaminated with $CuCl_2$ were found to adsorb moisture dependent upon the amount of contamination placed on the surface.[16] The substrate with an order of magnitude greater mass of contaminants also adsorbed an order of magnitude greater mass of water.

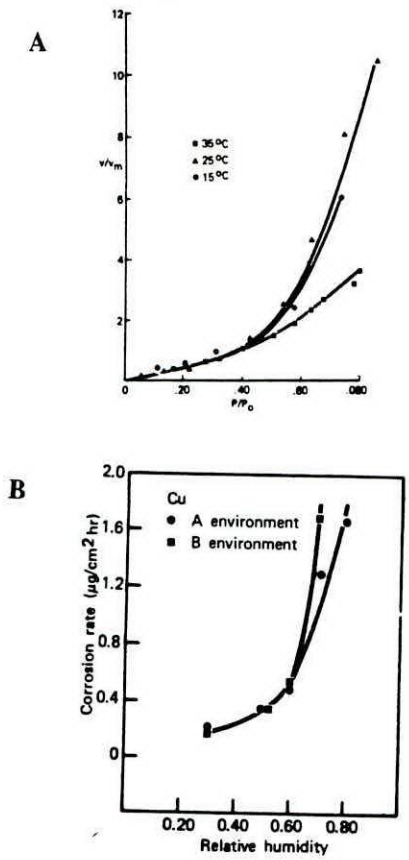

FIGURE 3: **Influence of Relative Humidity as Determined by D.W. Rice *et.al.* A) Monolayers of Water Adsorbed on Co [14] B) Corrosion of Cu [6]**

Although the amount of water adsorbed on a material is frequently expressed in terms of "equivalent monolayers", real surfaces have a roughness much greater than the thickness of these adsorbed "layers". Thus, the potential for heterogeneous adsorption of the water exists. Such behavior would encourage the variation of corrosion product thicknesses on a microscopic scale. K.-J. Eichhorn and W. Forker linked their observations of heterogeneous SO_2 adsorption to the possibility of heterogeneous water adsorption.[17] Indeed, the action of humidified sulfur dioxide on copper has been shown by transmission electron microscopy to produce pits and protrusions on the order of 50-100 nm in diameter.[18]

PHYSICAL CHEMISTRY OF ELECTROLYTE

With the adsorption of water from the surrounding environment and the supply of corrosive species to the surface either through gas phase transport or from pre-existing contamination, a corrosive electrolyte is formed. The composition of this solution is determined by the flux of species from the surrounding environment and their respective solubilities. Using a combination of quartz crystal microbalance and ion chromatographic techniques, J.F. Dante and R.G. Kelly found nitrate to dominate the electrolyte formed on gold exposed to 264 ppb NO_2 in a humid environment.[19]

The species which become incorporated in the thin film electrolyte can encourage the growth of a layer of corrosion products in several different ways. Gases such as SO_2, NO_2, and H_2S are capable of acidifying the solution, thereby increasing the corrosivity. The pH will then be determined by the concentration of these species within the solution. Based upon thermodynamic calculations, S.K. Chawla and J.H. Payer indicated that 100 ppb SO_2 should produce an electrolyte dominated by the HSO_3^- ion with a pH of 4.5.[20] As these ionic species undergo incorporation into the thin electrolyte film, they will increase the solution conductivity and, potentially, the corrosion rate.

In addition to controlling the acidity of solution, gaseous and particulate sources contribute various species, such as chlorides, which are capable of breaking down protective oxide films. The ionic constituents of the electrolyte can also play a role by participating in many possible redox reactions. Hence, the addition of a cathodic depolarizer can increase the corrosion current and become a constituent in the growing film. S.K. Chawla, B.I. Rickett, and J.H. Payer have found this process to occur for the reaction between copper and moist sulfur dioxide. As indicated by x-ray photoelectron spectroscopic analysis (XPS), the resulting tarnish film was composed of cuprous oxide and a small amount of copper sulfide which would have required the reduction of sulfur (+IV) to sulfur (-II).[21,22] Further knowledge of the action of these gases individually and in combination is important as certain mixtures have been shown to function in a synergistic manner, such as the behavior exhibited by sulfur dioxide and nitrogen dioxide on nickel.[23] XPS

analysis has indicated the formation of significant amounts of cupric species, as CuO and $Cu(OH)_2$, upon exposure of copper to a 75% relative humidity and 23°C gas mixture containing 75 ppb SO_2 and 120 ppb NO_2.[22]

With the growth of a corrosion product layer, the concentration of various species will change as a function of location and time in the solution. This process depends upon the consumption or production of species by the reactions taking place at the solution / substrate interface. The influence of transport parameters will play a large role in determining the amount of build up or depletion which occurs. Furthermore, with the removal of water from the surface during wet-dry cycling, the corrosivity of the solution will increase dramatically, allowing precipitation from solution at the relevant K_{sp} values.

FILM GROWTH PROCESSES

In the absence of an adsorbed electrolyte layer, metals are protected from further oxidation by a passive, native oxide film. Several different models have been advanced to describe the growth of a native oxide film on a metal surface in a bulk electrolyte. D.D. Macdonald summarized the Mott-Cabrera, Sato-Cohen, and Fehlner-Mott models for growth of passive oxides.[24] The Mott-Cabrera theory proposes metal cation transport with assistance from an electric field which was constant through the thickness of the film. Linking film growth to a coordinated flipping of oxygen and metal layers so as to create an oxide film structure, the Sato-Cohen model relies upon an alternative "place-exchange" mechanism. The Fehlner-Mott model alters the Mott-Cabrera model to account for film growth by anion diffusion and to place the rate limiting step for reaction at the film / solution interface. Macdonald has advanced a point defect model to account for passive film formation with continued oxide growth dependent upon the transport of vacancy sites.[25] As proposed, the steady state would be reached when the film formation reactions balanced the film dissolution reactions. Other researchers have presented theories for the passive film formation processes controlled by cation and anion vacancy mechanisms with the current dependent upon the vacancy concentration.[26,27]

Before tarnish film structures can form on the surface of a material, the native oxide film must be altered or disrupted in some manner to allow further oxidation of the underlying metallic substrate. Two mechanistic possibilities for this disruption exist. One process involves dissolution of the dense native oxide film and replacement with a precipitated, porous film structure. Alternatively, the native oxide could remain in place on the surface, undergoing a structural modification which would permit transport of the species necessary for growth of a tarnish film. Nordstrom has asserted that precipitated products will be characterized by fine, amorphous particles; whereas, product formation by a sorption process will create crystalline structures.[28]

The composition and structure of the growing product layer will control the corrosion rate and the subsequent appearance of a terminal film thickness. Growth of the initial film into more advanced stages depends upon the continued transport of species to the reaction interface. Certain factors can influence the observed transport properties. Macdonald has indicated that vacancy flux, thus mass transport, through a film could be increased by the action of chloride ions.[24] Likewise, as many tarnish films are characterized by non-stoichiometric, ionically conductive structures, illumination of a material could alter the electronic and ionic transport properties and, thus, the corrosion rate.

METALLURGY OF THE UNDERLYING METALLIC SUBSTRATE

The metallurgy of the substrate subjected to environmental attack can influence the composition and rate of formation of the product layer. Obviously, the particular composition of a material has a direct impact upon the process. Copper experiences tarnishing; whereas, gold is immune. Alloying can dramatically alter normal film growth characteristics by supplying an element which either segregates to the surface and forms a more protective oxide or becomes incorporated in the native oxide film as a dopant, thereby altering the film transport properties. G. W. Kammlott *et.al.* found that the severity of H_2S attack was one or two orders of magnitude worse for copper than for various brass compositions.[29]

The structure of the substrate also determines the impact of environmental attack. J.G. Bornstein *et.al.* found significant differences between the corrosion behavior of planar magnetron sputtered and electroplated Ni-Fe thin films. The electroplated films acted as though iron-rich, whereas the sputter deposited films displayed nickel-rich characteristics.[30] Mechanical working or residual stresses can severely

impact the reactivity of the substrate by providing a high energy surface containing a large number of defects and dislocations. Even crystallographic orientation can influence the oxidation rate of a metallic substrate.[31]

EXTERNAL STRESSES - MECHANICAL, THERMAL, GALVANIC, AND ELECTRICAL FIELD

Several external variables can affect the environmental attack of electronic materials and devices, including: mechanical, thermal, galvanic, and electrical field stresses. The presence of mechanical stress between two components at a solder joint can encourage a stress corrosion cracking phenomena. Mechanical parameters can also appear as fretting corrosion with the relative displacement which occurs between two mated surfaces continually breaking down any protective oxide layers.

The temperature of the surrounding environment can also play a significant role. Obviously, the kinetics of interfacial reactions, solid state transport through the tarnish film, and pollutant solubility in the thin adsorbed electrolyte will be controlled by thermal considerations. Interestingly, it has been found for temperature regimes near ambient that the amount of water adsorbed as a function of relative humidity is largely independent of temperature.

The coupling of dissimilar metals or the biasing of components within close proximity can accelerate attack by creating well defined cathodic and anodic sites. N.A. Stennett *et.al.* observed two to three times greater corrosion for powered contacts subjected to a severe environment (200 ppb H_2S, 50 ppb Cl_2, 200 ppb NO_2, 75% RH, and 50°C) than were observed for unpowered contacts subjected to the same conditions.[32] Similarly, M. Iannuzzi and R.P. Kozakiewicz found that anodic biasing increased corrosion rates and that galvanic coupling at a gold / aluminum wire bond accelerated the corrosion of the aluminum.[33]

PREDICTING AND PREVENTING ENVIRONMENTAL ATTACK

ACCELERATED TESTING AND LIFETIME PREDICTION

The parameters mentioned in the previous section interact to control the rates and mechanisms of the environmental attack on electronic materials. Within actual service environments a great variability arises as to the relative importance of each of these parameters. For example, one site may be extremely susceptible to particulate deposition, whereas another location may be subjected primarily to high pollutant gas concentrations. This complex interaction of environmental parameters makes the prediction of lifetimes for electronic components extremely difficult.

In order to subject coupons to well defined environmental conditions, chambers have been designed which permit careful control over many exposure variables, including pollutant gas concentrations, temperature, relative humidity, flow rate, particulate deposition, mechanical contact between mating connectors, biasing of conduction lines, and illumination.[12,22,34,35] Attempts to mimic the compositions and thicknesses found for field exposures have been difficult as a result of the large number of interacting variables. A better understanding of the role of individual parameters, such as the mechanism by which increasing relative humidity increases the observed tarnishing rate, will permit better implementation of accelerated testing programs. Without a basic understanding of these roles, the selection of acceleration factors and the alteration of environmental parameters to produce accelerated exposures are problematic. Improper criteria could dramatically shift the composition and/or growth mechanisms away from those active for field coupons.

Models have been developed to evaluate the influence of various exposure parameters upon observed behavior with the ultimate goal of providing information for the basis of prediction. Thermodynamic calculations have been utilized to explain the formation of particular film compositions. E. Mattsson has approached the atmospheric corrosion of steel, zinc, aluminum, and copper with potential-pH and concentration-pH diagrams.[36] The diagrams were utilized to support observations of stable, basic copper chlorides in the presence of a marine atmosphere. Thermodynamic considerations have also been applied to the prediction of thin, adsorbed electrolyte film chemistries.[20,37] Of course, kinetic factors play a role as well and can cause deviations from the expected outcome.

Models have also been developed along empirical lines. S.P. Sharma *et.al.* developed an accelerated test which consists of high / low temperature and relative humidity cycling.[38] The acceleration factor for these exposures was based

upon a kinetic equation which takes into account relative humidity and temperature. Others have developed relative humidity / temperature plots which define contours of equal failure risk.[39] Unfortunately, the large number of interacting variables make this approach extremely difficult, as a particular model may fail to take into account all of the relevant parameters.

APPROACHES TO MINIMIZING DAMAGE

The methods available for minimizing environmental attack can be grouped into the following five basic categories: modification of the environment, application of a coating or barrier layer, selection of an alternate material, redesign of the component, and alteration of the electrochemical potential.[40] With the exception of controlling the electrochemical potential of a component, one or more of these traditional techniques can be applied to the protection of electronic materials. As these materials are electrically powered by design, the application of anodic or cathodic protection schemes to these structures is often not applicable.

Successful control of environmental attack requires the reduction of the availability of the moisture, pollutant gases, and particulates necessary to support electrochemical corrosion. Electronic enclosures, conditioning or treatment of the air supply, and relocation of electronic packages to more benign environments all serve to accomplish this goal. Yet, with the increasing severity of the "typical" service environment, this option has become much less feasible. The application of a coating or barrier layer also functions to reduce environmental attack by separating the susceptible metallic substrate from the available moisture and pollutants. This approach has the additional advantage of becoming a protective element transported with the overall electronic package into the service environment. Yet, as connections must be made between the conduction pathways of mated devices, some parts and surfaces will be exposed by necessity.

Improving the resistance of a component to environmental stress through a redesign process can include provision for greater corrosion tolerances, incorporation of redundant electronic functions, and minimization of the amount of susceptible material. Obviously, design considerations are primarily dictated by the size and electrical function of the device, and these parameters often lie counter to those considered ideal from the perspective of corrosion control.

A final method for minimizing the damage caused by environmental factors lies in the ability to modify or change the composition and structure of the material under attack. Alloying an existing material can result in greatly improved resistance to attack. Alternatively, an entirely new material can be developed. Proper selection can provide a material with either a greater intrinsic nobility or a more robust passive film. Control over parameters such as the grain size and morphology, surface roughness, and deposition conditions can provide the characteristics necessary to improve the reliability of electronic materials subjected to environmental stresses.

SUMMARY

This paper has touched upon some of the issues important to understanding the influence the environment can have on the reliability of electronic materials, including: the sources of environmental attack, the phenomenology of failure, the controlling environmental parameters, the prediction of component lifetimes, and the methods for preventing environmental attack. A multifaceted experimental approach is necessary to elucidate the chemistry, structure, and growth mechanisms relevant to the corrosion products formed on electronic materials in harsh service environments. The information gathered from such studies will reveal strategies for locating, predicting, and minimizing environmental attack.

ACKNOWLEDGEMENTS

This work was partially supported by NSF Grant No. DMR-9015475 and by IBM Shared University Research Program Grant No. 1314. B.I. Rickett acknowledges the support of a National Science Foundation graduate fellowship.

REFERENCES

1. J.H. Payer, "Effect of Environmental Stress on Reliability of Automotive Electronics", Paper 405, *Corrosion '91*, National Association of Corrosion Engineers, Cincinnati, Ohio (1991).

2. A.J. Raffalovich, *IEEE Transactions on Parts, Hybrids, and Packaging*, PHP-7, No.4, 155-162 (1971).

3. D.A. Jeannotte, L.S. Goldmann, and R.T. Howard, in *Microelectronics Packaging Handbook*, R.R. Tummala and E.J. Rymaszewski, eds., Van Nostrand Reinhold, New York, 276 (1989).

4. S.K. Chawla and J.H. Payer, "Atmospheric Corrosion: A Comparison of Indoor vs. Outdoor", *11th International Corrosion Conference*, Florence, Italy, 1990.

5. E. Mattsson, *Materials Performance*, 21, No.7, 9-19 (1982).

6. D.W. Rice, P. Peterson, E.B. Rigby, P.B.P. Phipps, R.J. Cappell, and R. Tremoureux, *J. Electrochem. Soc.*, 128, 275-284 (1981).

7. D.W. Rice, R.J. Cappell, W. Kinsolving, and J.J. Laskowski, *J. Electrochem. Soc.*, 127, 891-901 (1980).

8. S. Zakipour and C. Leygraf, *J. Electrochem. Soc.*, 133, 21-30 (1986).

9. T.E. Graedel, *Corrosion Science*, 27, 721-740 (1987).

10. J.D. Sinclair, *J. Electrochem. Soc.*, 135, 89C-95C (1988).

11. J.D. Sinclair, L.A. Psota-Kelty, and C.J. Weschler, *Atmospheric Environment*, 19, No.2, 315-323 (1985).

12. L. Volpe and P.J. Peterson, *Corrosion Science*, 29, 1179-1196 (1989).

13. J.D. Sinclair, *J. Electrochem. Soc.*, 135, 89C-95C (1988).

14. D.W. Rice, P.B.P. Phipps, and R. Tremoureux, *J. Electrochem. Soc.*, 126, 1459-1466 (1979).

15. S.P. Sharma, *J. Vac. Sci. Technol.*, 16, No. 5, 1557-1559 (1979).

16. G.W. Warren and I. Chatterjee, *"An Analysis of the Moisture Adsorption Process: Important Parameters and Investigative Techniques"*, **private communication.**

17. K.-J. Eichhorn and W. Forker, *Corrosion Science*, 28, 745-758 (1988).

18. S.K. Chawla and J.H. Payer, *J. Electrochem. Soc.*, 137, 60-64 (1990).

19. J.F. Dante and R.G. Kelly in *Symposium on Corrosion and Reliability of Electronic Materials and Devices, The Electrochemical Society 182nd Meeting*, Toronto, Canada (1992) **in press.**

20. S.K. Chawla and J.H. Payer, *Corrosion*, 46, No.10, 860-865 (1990).

21. S.K. Chawla, B.I. Rickett, and J.H. Payer in *Corrosion of Electronic and Magnetic Materials, ASTM STP 1148*, P.J. Peterson, ed., American Society for Testing and Materials, Philadelphia, 21-35 (1992).

22. B.I. Rickett and J.H. Payer in *Symposium on Corrosion and Reliability of Electronic Materials and Devices, The Electrochemical Society 182nd Meeting*, Toronto, Canada (1992) **in press.**

23. S. Zakipour, C. Leygraf, and G. Portnoff, *J. Electrochem. Soc.*, 133, 873-876 (1986).

24. C.Y. Chao, L.F. Lin, and D.D. Macdonald, *J. Electrochem. Soc.*, 128, 1187-1198 (1981).

25. D.D. Macdonald and M. Urquidi-Macdonald, *J. Electrochem. Soc.*, 137, 2395-2402 (1990).

26. R. Kirchheim, *Corrosion Science*, 29, 183-190 (1989).

27. G.T. Croft and D. Tuomi, *J. Electrochem. Soc.*, 108, 915-922 (1961).

28. D.K. Nordstrom, *Geochim. Cosmochim. Acta.*, 46, 681-692 (1982).

29. G.W. Kammlott, J.P. Franey, and T.E. Graedel, *J. Electrochem. Soc.*, 131, 505-510 (1984).

30. J.G. Bornstein, C.H. Lee, L.A. Capuano, and D.A. Stevenson, *J. Appl. Phys.*, 65, No.5, 2090-2094 (1989).

31. A.T. Gwathmey and K.R. Lawless in *The Surface Chemistry of Metals and Semiconductors*, H.C. Gatos *et.al.*, eds., John Wiley & Sons, New York, 483-521 (1960).

32. N.A. Stennett, T.P. Ireland, and D.S. Campbell, *Proceedings of the Thirty-Sixth IEEE Holm Conference on Electrical Contacts and the Fifteenth International Conference on Electrical Contacts*, Montreal, Canada, 174-181 (1990).

33. M. Iannuzzi and R.P. Kozakiewicz, *Proceedings of the Thirty-Second Electronic Components Conference*, IEEE, San Diego, CA, 391-400 (1982).

34. W.J. Curren, J.R. Martin, and P. Gilson, "Design and Operating Characteristics of a Mixed Gas Environmental Chamber", Paper 326, *Corrosion '85*, National Association of Corrosion Engineers, Boston, Massachusetts (1985).

35. J.L. Chao and R.R. Gore, *Proceedings of the Thirty-Seventh IEEE Holm Conference on Electrical Contacts*, Chicago, Ill., 216-228 (1991).

36. E. Mattsson, *Materials Performance*, 21, No.7, 9-19 (1982).

37. M.Carballeira, A. Carballeira, J.Y. Gal, *"Contribution to the Study of Corrosion Phenomena in Industrial Atmosphere Thermodynamic Approach"*, **private communication.**

38. S.P. Sharma, J.H. Thomas, and F.E. Bader, *J. Electrochem. Soc.*, 125, 2002-2004 (1978).

39. G.F. Cerofolini and C. Rovere, *Thin Solid Films*, 47, 83-94 (1977).

40. M.G. Fontana in *Corrosion Engineering, 3rd edition*, McGraw-Hill Book Co.: New York, 278-316 (1986).

Table I. Inorganic pollutants used in this study, typical indoor and outdoor ranges, analytic methods, and rationale for selection

Pollutant gas	Typical outdoor range (μg/m³) (18, 29)	Typical indoor range (μg/m³) (18)	Analytic methods	Rationale for selection
SO_2	3-185	1-40	Flame photometric, (continuous) (22), West Gaeke (23) (periodic)	Major pollutant, known to attack many metals. Forms acidic surface
NO_2	20-160	3-60	Chemiluminescence, (continuous) (24), Saltzman (periodic) (25)	Major pollutant, known to attack Co, Ni, and Fe (18)
H_2S	1-36	0.2-1	Lead acetate tape sampler with prefilter (periodic) (26)	Stress corrosion accelerator, known to attack Cu and Ag
O_3	10-80	7-45	Chemiluminescence (continuous) (27)	Major pollutant, degrades polymers and accelerates oxidation of H_2S, NO_2, and SO_2
HCl	0.2-5	0.08-0.3	O-tolidine densitometry (periodic), $AgNO_3$ titration (periodic)	Destabilizes passive films by lattice impregnation and acid dissolution
Cl_2	Less than 5% of HCl levels except where local Cl_2 source exists	0.004-0.015	Same as above	Same as above
NH_3	6-12	10-150	Chemiluminescence (continuous) (28)	Major pollutant, forms complexes with Cu and Ag, forms basic surface

indoor air over the samples at 2.5 m/sec parallel to the surface. The location and characteristics of the eight indoor test sites in this study are given in Table II. Samples were returned after 6, 12, and 18 month exposure and reweighed after removing benzene soluble organic deposits. These organic deposits generally were only 10%-20% of the inorganic weight gain; however, for a few samples they were comparable. Pollutant and humidity measurements were concurrently measured at six of the eight sites. This data has been summarized previously, as has the high resolution x-ray photoelectron spectroscopic analysis of the corrosion product on the samples returned after 18 months (18).

Results and Discussion

Relative humidity.—The corrosion rate, r, dependence on relative humidity, RH, for both copper and silver in two complex test environments are shown in Fig. 2. Pollutant concentrations in these tests are listed in Table III. The rates are the initial linear rate constants. These were chosen because the total weights are more representative of the field measurements. These rates will generally overestimate the amount of weight increase for long test times; however, the same general dependence on atmospheric variables will be observed. Figure 3 shows representative weight gain *vs.* time curves at various relative humidities for copper.

The difference between copper and silver is remarkable. The corrosion rate of copper is strongly dependent on relative humidity. The approximate equation relating rate and relative humidity is $r = 0.042 \exp 4.6RH$ for environment A with a correlation coefficient equal to 0.97. Environment B results in a rate that is more sensitive to RH. These results are generally in agreement with the work of Vernon (8) and others (1-5) at higher pollutant concentrations. Corrosion rates could be measured over the entire range of RH's studied. There was no "critical humidity" in an absolute sense. At high SO_2 concentrations or in SO_2 environments only, where equilibrium with sulfate surface products

Table II. Field site physical characteristics

Site	Location	Outdoor environment	Air conditioned
1	Los Angeles, CA	Urban	Yes
2	Chicago, IL	Urban	Yes
3	Manhattan, New York City	Urban	Yes
4	Houston, TX	Industrial/rural	Yes
5	North Indiana	Industrial	Yes
6	South Carolina	Industrial	Yes
7	New Jersey	Industrial	No
8	New Jersey	Industrial	No

Table III. Composition of the complex accelerated laboratory test environments. ($T = 25°C$, $v = 0.36$ M/sec)

Pollutant	Concentration (μg/m³) Environment A	Environment B
SO_2	810	860
NO_2	940	990
O_3	334	0
NH_3	0	0
Cl_2	8.4	8.4
HCl	0	16.8
H_2S	21	54

or condensed sulfuric acid controls the amount of adsorbed water, the idea of a critical humidity may be useful. For complex environments, care must be taken in using the critical humidity concept without a precise understanding of the corrosion products. The atmospheric corrosion mechanism for copper is electrochemical with the water-pollutant chemistry providing the medium for ionic mobility and surface product dissolution. There are many surface reactions that are thermodynamically favorable for copper oxidation.

Silver, unlike copper, shows no significant rate dependence on relative humidity, $r = 0.37 \exp 0.13RH$, in these complex environments. This is evidence that aqueous electrochemical intermediates have different roles in the mechanism of silver and copper corrosion.

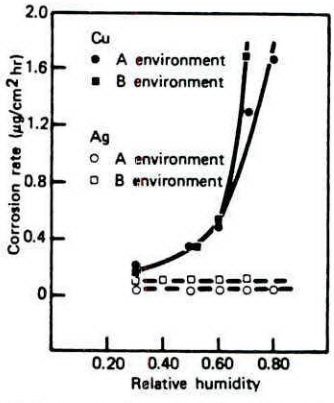

Fig. 2. Corrosion rate of copper and silver vs. relative humidity in two test environments.

The upper spectrum is that of cobalt film exposed to laboratory air at 50% RH for many days. Only a small cobalt metal satellite is seen, but both oxygen associated with an oxide (529.5 eV) and hydroxide (531.5 eV) are seen. After 240 sec of Ar ion sputtering or approximately 0.8 nm material removal, a large cobalt metal peak is apparent as well as a dominant O(1s) oxide peak. Continued Ar sputtering completely removes all oxygen and leaves only a metallic cobalt surface. Final exposure of the cobalt metal surface to 1500 sec of 760 Torr air at 50% RH again shows a dominant high BE O(1s) peak, conjectured to be $Co(OH)_2$, and the emergence of a Co(2p3/2) peak due to oxidation.

The rapid removal of the O(1s) peak associated with the hydroxide and the emergence of the cobalt metal peak in spectrum b suggest the hydroxide is reduced directly to the metal rather than through an oxide intermediate, i.e., the cobalt hydroxide bond is weaker than the oxygen hydrogen bond. Furthermore, spectrum d suggests the rapid initial surface reaction on cobalt is hydroxide formation. Subsequently, an oxide forms by either hydroxide dissociation or oxygen interaction. In any case, the cobalt surfaces that initiate corrosion and adsorb H_2O are predominately complex hydroxylated structures.

H_2O adsorption.—The adsorption of H_2O on these complex hydroxylated cobalt surfaces is characterized by the isotherms measured at three temperatures shown in Fig. 2. These isotherms are typical of those seen on hydroxylated Fe_2O_3 particles (20). Figure 3 shows the isotherms plotted *vs.* p/p_o, the relative humidity. The isotherms exhibited no hysteresis, suggesting no chemisorption during the H_2O exposures. The surfaces had previously been exposed to enough H_2O, as the surface studies demonstrated, to preclude any further chemisorption. The amount of adsorbed H_2O was normalized when plotted against p/p_o up to approximately 0.50 RH. This is characteristic of gas-solid interactions (21). The isotherms also show that on cobalt many apparent monolayers of water are present at higher RH's. It is not surprising that corrosion should proceed readily via these relatively thick layers of water on the hydroxy surfaces.

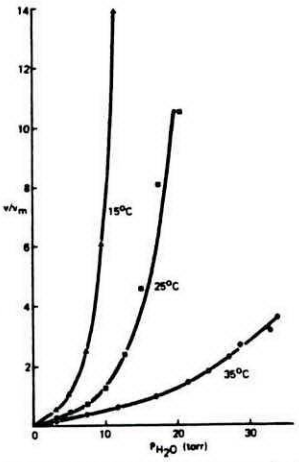

Fig. 2. Adsorption isotherms of H_2O on evaporated cobalt thin film surfaces. The ratio of the adsorbed volume of water to the volume of a monolayer of water (v/v_m) is plotted *vs.* the pressure of H_2O.

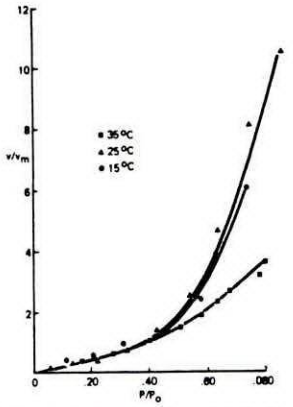

Fig. 3. Adsorption isotherms of H_2O on cobalt thin film surfaces. The ratio of the adsorbed volume to the volume of a monolayer of water (v/v_m) is plotted *vs.* the relative humidity (p/p_o).

Table II summarizes the heat of adsorption (ΔH_{ad}), monolayer volume, and relative humidity at apparent monolayer coverage obtained by fitting the data to a BET isotherm over the interval p/p_o = 0-0.4. The heat of vaporization (ΔH_v) of water was taken as 10.5 kcal/mole in these calculations. The similarity between the ΔH_{ad} and ΔH_v implies that the H_2O molecule shows no great preference for the surface as compared to liquid water. It could just as well combine with a neighboring H_2O molecule to form a local H_2O cluster. The ΔH_{ad} measured in this study on cobalt is slightly less than that reported on Fe_2O_3 particles (20), Cu surfaces (22), and Au surfaces (22), but in general agreement. Klier *et al.* have demonstrated that water clusters on surfaces well below apparent monolayer coverage (23). In fact, they found via infrared spectroscopy that silica surfaces at monolayer H_2O coverage consisted of equivalent amounts of clustered and surface adsorbed water. These results suggest that the apparent monolayer coverage, as measured in the isotherms for cobalt, may significantly underestimate the local surface volume of H_2O due to clustering.

To develop this morphology theme further, we exposed Co thin films on TEM grids for short periods of time to the reference atmosphere (Table I). This was thought to be a good way to fingerprint where H_2O was or at minimum where corrosion initiated. A representative micrograph at 50,000× magnification of a sample exposed for 18 hr shows a profound hierarchy of phenomena in Fig. 4. The dark regions are more dense or thicker and adsorb more electrons in this positive TEM image. The surface is clearly corroding in a very heterogeneous way. Small nucleation sites consisting of excess Cl^- are distributed uniformly over the surface with an areal density of 24×10^8 nuclei/cm², a radius of 50 nm, and a center-to-center spacing equal to 200 nm. These nuclei are

Table II. Heats of adsorption (ΔH_{ad}), relative humidity (RH) at monolayer coverage, and monolayer volume for H_2O on air exposed Co surfaces

T (°C)	ΔH_{ad} (kcal/mole)	$RH\left(\frac{p}{p_m}=1\right)$	v_m (cm³/cm²)
15	11.1	0.38	2.79×10^{-4}
25	11.0	0.38	3.90×10^{-4}
35	11.0	0.38	2.91×10^{-4}